



UNIVERSIDADE DE COIMBRA

Mestrado em Física Nuclear e de Partículas
Faculdade de Ciências e Tecnologia

**Combined effects of strong and
electroweak effective FCNC operators in
top production at the LHC**

Miguel Daiyen Carvalho Won

Supervisor: Doutor Rui Alberto Serra Ribeiro dos Santos
Co-Supervisor: Professor Doutor António Joaquim Onofre de Abreu
Ribeiro Gonçalves

July 2008

Acknowledgements

First I want to thank both my supervisors, Doutor Rui Alberto Serra Ribeiro dos Santos from Department of Physics, Royal Holloway at University of London, and Professor Doutor António Joaquim Onofre de Abreu Ribeiro Gonçalves from Physics Department at the University of Coimbra. Their help and enthusiasm was extremely relevant for this thesis as well as for my general academic and scientific formation. I also thank to everyone involved in this work, in particular to Pedro Ferreira, Orlando Oliveira, Renato Guedes and Rita Coimbra, without whom I hardly would have reached this final stage. Finally thanks to all my office colleagues that supported me in everyday details with patience and kindness.

The work presented in this thesis was supported by FCT through the project POCI/FP/81950/2007.

Contents

1	Introduction	1
2	Theoretical background	5
3	Single top Production	9
3.1	Process 1	12
3.1.1	Results	20
3.2	Processes 6 to 8	22
3.2.1	Process 6	22
3.2.2	Results	25
4	From partons to protons	27
4.1	PDF	27
4.2	Kinematical limits	28
5	Results and discussion	31
5.1	Processes 1 to 5	31
5.2	Processes 6 to 8	41
6	Conclusions	43
A	Processes 2 to 8	45
A.1	Process 2	45
A.2	Process 3	47
A.3	Process 4	52
A.4	Process 5	54
A.5	Process 7	56
A.6	Process 8	58

B	Mathematica	61
	B.0.1	Transition amplitudes calculations 61
	B.0.2	PDF integration 62
C	Standard Model Feynman Rules	67

List of Figures

1.1	SM top decay diagram.	2
1.2	FCNC top decay diagram.	2
1.3	Cross sections for the processes $pp \rightarrow t + jet$ (crosses) and $pp \rightarrow t + W$ (stars) via an u quark, as a function of the branching ratio $BR(t \rightarrow gu)$. Plot from [3].	3
2.1	Feynman rules for anomalous $g\bar{u}_i t$ and $g\bar{t}u_i$	7
2.2	Feynman rules for anomalous $\gamma\bar{u}_i t$ and $\gamma\bar{t}u_i$	8
2.3	Feynman rules for anomalous $Z\bar{u}_i t$ and $Z\bar{t}u_i$	8
3.1	Feynman diagrams of $qq \rightarrow tq$ process for the strong sector.	9
3.2	Feynman diagrams of $qq \rightarrow tq$ process for the electroweak sector.	10
3.3	Feynman diagrams of $q\bar{q} \rightarrow t\bar{q}$ process for the strong sector.	10
3.4	Feynman diagrams of $q\bar{q} \rightarrow t\bar{q}$ process for the electroweak sector.	10
3.5	Momentum convention.	11
3.6	Feynman diagrams for $u^b u^b \rightarrow t^b u^b$ process.	15
3.7	Feynman diagrams for $u^b u^y \rightarrow t^b u^y$ (t channel) and $u^b u^y \rightarrow t^y u^b$ (u channel) processes.	15
3.8	Feynman diagrams for $u^y u^b \rightarrow t^y u^b$ (t channel) and $u^y u^b \rightarrow t^b u^y$ (u channel) processes.	16
3.9	Feynman diagrams for $u^y u^y \rightarrow t^y u^y$ process.	16
3.10	FCNC Feynman diagram of process 6 for the strong sector.	23
3.11	FCNC Feynman diagram of process 6 for the electroweak sector.	23
3.12	SM Feynman diagram for process 6.	23
4.1	Pictorial view of a collision at the LHC.	27
4.2	Quarks up, down, charm and gluon PDF functions for CTEQ5M. Plots from [11].	29

5.1	Cross section for the processes $qq \rightarrow tq$ as a function of the branching ratio $BR(t \rightarrow qg)$	33
5.2	Cross section for the processes $qq \rightarrow tq$ as a function of the branching ratio $BR(t \rightarrow q\gamma)$	33
5.3	Cross section for the processes $qq \rightarrow tq$ as a function of the branching ratio $BR(t \rightarrow qZ)$	34
5.4	Cross section for the processes $qq \rightarrow tq$ as a function of the branching ratio $BR(t \rightarrow qX)$. The X particle can be a gluon, a photon or a Z.	35
5.5	Cross section for the processes $qq \rightarrow tq$ as a function of the branching ratio $BR(t \rightarrow qX)$ rescaled.	35
5.6	Gluon processes cross section as a function of the $BR(t \rightarrow qg)$	37
5.7	Total cross section for the processes $pp \rightarrow t + jet$ as function of the branching ratio $BR(t \rightarrow qg)$	37
5.8	Total cross section for the processes $pp \rightarrow t + jet$ as function of the branching ratio $BR(t \rightarrow q\gamma)$	38
5.9	Total cross section for the processes $pp \rightarrow t + jet$ as function of the branching ratio $BR(t \rightarrow qZ)$	38
5.10	Total cross section for the processes $pp \rightarrow t + jet$ as function of the branching ratio $BR(t \rightarrow qX)$. The X particle is a gluon, a photon or a Z.	39
5.11	Strong sector cross section for processes $qq \rightarrow tq$ as a function of the branching ratio $BR(t \rightarrow qg)$	40
5.12	Electroweak and interferences sector cross section for processes $qq \rightarrow tq$ as a function of the branching ratio $BR(t \rightarrow qY)$. The Y particle can be a photon or a Z.	41
5.13	Cross section for processes $qq \rightarrow tq$ as a function of the branching ratio $BR(t \rightarrow qg)$. Processes with b quarks as final products were not considered.	42
5.14	Cross section for processes $qb \rightarrow tb + q\bar{b} \rightarrow t\bar{b}$ as a function of the branching ratio $BR(t \rightarrow qg)$	42
A.1	Feynman diagram of process 2 for the strong sector.	45
A.2	Feynman diagram of process 2 for the electroweak sector.	45
A.3	Feynman diagram of process 3 for the strong sector.	47
A.4	Feynman diagram of process 3 for the electroweak sector.	47
A.5	Feynman diagram of process 4 for the strong sector.	53
A.6	Feynman diagram of process 4 for the electroweak sector.	53
A.7	Feynman diagram of process 5 for the strong sector.	55
A.8	Feynman diagram of process 5 for the electroweak sector.	55

A.9	FCNC Feynman diagram of process 7 for the strong sector.	56
A.10	FCNC Feynman diagram of process 7 for the electroweak sector.	56
A.11	SM Feynman diagram for process 7.	57
A.12	FCNC Feynman diagram of process 8 for the strong sector.	59
A.13	FCNC Feynman diagram of process 8 for the electroweak sector.	59
A.14	SM Feynman diagram for process 8.	59
B.1	Trace calculation section.	62
B.2	Mathematica file for gluon channel of process 1.	63
B.3	Section of amplitudes calculation results.	64
B.4	Mathematica file of the PDF integration for <i>process1</i>	65
B.5	Second integration section of the PDF integration.	66
C.1	Feynman rules for the SM $\bar{u}ug$ and $\bar{d}dg$ vertices. λ^a are the Gell-Mann matrices normalized such as $Tr(\lambda^a \lambda^b) = 2\delta^{ab}$	67
C.2	Feynman rules for the SM $\bar{u}u\gamma$ and $\bar{d}d\gamma$ vertices.	67
C.3	Feynman rules for the SM $\bar{u}dW^+$ vertex.	68
C.4	Feynman rules for the SM $\bar{u}uZ$ and $\bar{d}dZ$ vertices. $T_3 = 1/2$ for up-type quarks and $T_3 = 1/2$ for down-type quarks	68

List of Tables

1.1	Expected quark top decay branching ratios for several physical models. Table from [4].	2
1.2	Possible channels for single-top production with FCNC. Table from [5].	4
3.1	FCNC single-top production processes considered.	11
3.2	Kinematics constrains.	12
3.3	Anomalous constants from the Gluon, Photon, and Z channel results.	20
3.4	Anomalous constants from the Gluon-Photon, Gluon-Z and Photon-Z channel results.	21
3.5	Anomalous constants from the Gluon-W, Photon-W and Z-W channel results.	25
5.1	Cross section contributions of the different sectors for one specific point.	40
5.2	Branching ratios for one specific point.	41

Chapter 1

Introduction

One of the main characteristics of the Large Hadron Collider (LHC), is the ability to produce a large number of top quarks. In the regime of low luminosity 8 million top quark pairs per year and per experiment are anticipated. Since this quark is the least studied in the Standard Model (SM), due to the current lack of data, this new accelerator will be an excellent laboratory to study physics beyond the SM associated to this sector.

In the present work we study flavour changing neutral currents (FCNC) associated with single-top quark production. This process is characterised by vertices where the current flavour changes and the charge is conserved. This kind of processes are, due to the Glashow-Iliopoulos-Maiani (GIM) mechanism, highly suppressed in the SM. In figures (1.1) and (1.2) we can see the top quark decay predicted by the SM and one example of an FCNC top decay, respectively. Although these FCNC processes are highly suppressed in the SM, there are some extensions like SUSY or multi-Higgs doublet models, that predict a very different FCNC decay branching ratios for the top quark. This can be seen in table (1.1). For the $t \rightarrow qg$ decay, an increase of eight orders of magnitude is expected for the branching ratio within SUSY, when compared to the expected SM value. For this reason, this decay is a good channel to test physics beyond the SM.

This work follows previous studies [1, 2, 3] where several cross sections for the FCNC in the strong sector were calculated and analysed. In table (1.2) the processes studied in those works is shown. In figure (1.3) the $pp \rightarrow t + jet$ cross section versus the branching ratio for the FCNC decay $t \rightarrow ug$ is presented. As we can see from figure (1.3) there is a significant contribution for the single-top production cross section, which implies that we are in the presence of a channel that is a good candidate for testing new

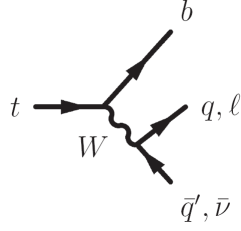


Figure 1.1: SM top decay diagram.

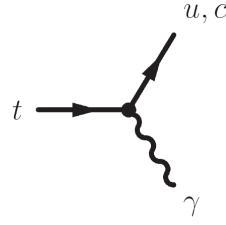


Figure 1.2: FCNC top decay diagram.

BR($t \rightarrow \text{FCNC}$) in several models:

	SM	QS	2HDM	FC 2HDM	MSSM	\tilde{R} SUSY
$t \rightarrow q\gamma$	$\sim 10^{-14}$	$\sim 10^{-9}$	$\sim 10^{-6}$	$\sim 10^{-9}$	$\sim 10^{-6}$	$\sim 10^{-6}$
$t \rightarrow qZ$	$\sim 10^{-14}$	$\sim 10^{-4}$	$\sim 10^{-7}$	$\sim 10^{-10}$	$\sim 10^{-6}$	$\sim 10^{-5}$
$t \rightarrow qg$	$\sim 10^{-12}$	$\sim 10^{-7}$	$\sim 10^{-4}$	$\sim 10^{-5}$	$\sim 10^{-5}$	$\sim 10^{-4}$

Table 1.1: Expected quark top decay branching ratios for several physical models. Table from [4].

physics at LHC.

From all the processes of table (1.2), we highlight the production processes $q\bar{q} \rightarrow t\bar{q}$ because there is an electroweak contribution to add to the strong one already calculated. This is not true for the remaining $pp \rightarrow t + \text{jet}$ channels. The strong channel contribution was calculated in [2]. The main objective of the present work is to complete the single-top production channel, which means to include the electroweak sector contribution and the interference terms between the two sectors. We started by cross-checking the calculation for the strong sector. We can now say that the single-top quark production through both the strong and electroweak channels is complete.

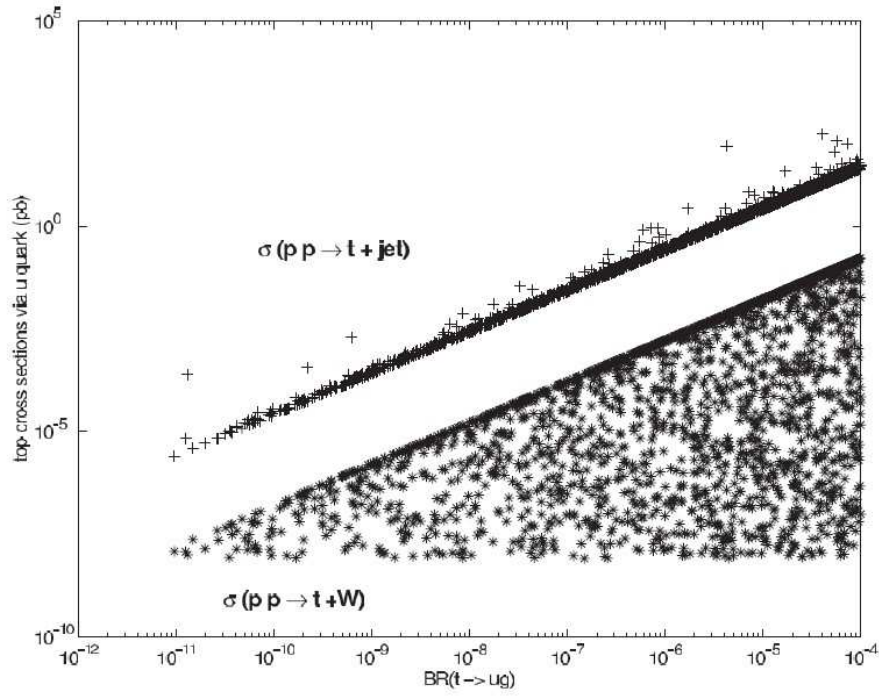


Figure 1.3: Cross sections for the processes $pp \rightarrow t + jet$ (crosses) and $pp \rightarrow t + W$ (stars) via an u quark, as a function of the branching ratio $BR(t \rightarrow gu)$. Plot from [3].

direct production	$pp \rightarrow (gq) \rightarrow t + X$
top + jet production	$pp \rightarrow (gg) \rightarrow \bar{q}t + X$ $pp \rightarrow (gq) \rightarrow gt + X$ $pp \rightarrow (\bar{q}q) \rightarrow \bar{q}t + X$ (including 4-fermion interactions)
top + anti-top production	$pp \rightarrow (gg) \rightarrow \bar{t}t + X$ $pp \rightarrow (\bar{q}q) \rightarrow \bar{t}t + X$
top + gauge boson production	$pp \rightarrow (gq) \rightarrow \gamma t + X$ $pp \rightarrow (gq) \rightarrow Zt + X$ $pp \rightarrow (gq) \rightarrow Wt + X$
top + Higgs production	$pp \rightarrow (gq) \rightarrow ht + X$

Table 1.2: Possible channels for single-top production with FCNC. Table from [5].

Chapter 2

Theoretical background

We can define an effective field theory (EFT) as a theory which aims to describe the main physical characteristics of a problem with respect to a domain of parameters. One of the common parameters used (it will be used in this work), is the energy scale of the physical problem. So in this example, one EFT is a physical theory that is supposed to work in a specific energy scale and does not try to explain physical interactions at higher energies. We can say that an EFT is not a model of physics that tries to describe some set of interactions at all energies scales, but a theory that describes the physics in one specific scale region. Like explained in [6], because of its richness, it is convenient to divide all physical phenomena in groups, so that it is not necessary (and probably is not possible) to explain everything at the same time. Doing this, we are dividing the physical domain into several regions. The theory which has the appropriate description of the important physics in each region, is called an effective theory, where appropriate means that there is no theory of everything that works for all physical domain and important means that the relevance of the physical phenomena is scale dependent.

The theoretical context of the present work uses this concept for the implementation of the FCNC processes. Just like previous works, the approach uses the effective operators formalism [7] in the attempt to introduce new relevant processes at higher energy scales. In this formalism the SM is considered as the low-energy effective theory and by "low-energy" we mean any process which occurs bellow the LEP energies. The effective Lagrangian technique was used, which means that the Lagrangian is written as a power expansion in $\frac{1}{\Lambda}$, where Λ is the scale parameter. In equation (2.1) we can see the form of this expansion. Since this scale factor has energy units, each Lagrangian term has to follows the dimension of Λ . Therefore, for the

first order of the expansion we have a dimension five Lagrangian and for the second order we have a dimension six one. For FCNC studies we have considered the expansion to the second order in $\frac{1}{\Lambda}$

$$\mathcal{L}_{eff} = \mathcal{L}^{SM} + \frac{1}{\Lambda}\mathcal{L}^{(5)} + \frac{1}{\Lambda^2}\mathcal{L}^{(6)} + O\left(\frac{1}{\Lambda^3}\right). \quad (2.1)$$

Each Lagrangian term is built from the combination of the fields under consideration. In the Buchmüller and Wyler formalism, fields are considered as classical and no additional fields are present. All Lagrangian terms considered here are $SU(3) \times SU(2) \times U(1)$ invariant. The $\mathcal{L}^{(5)}$ terms break baryon and lepton number conservation and usually are not considered. Therefore the remaining term which needs to be constructed is the dimension six term. The Lagrangian used in this work is taken from the vast list of dimension five operators of [7], and obeys specific criteria for the FCNC studies considered here. These are: they can not have impact on phenomena occurring at lower-energies and the operators chosen involve flavour changing interactions with a single top quark. Therefore we are searching, in the case of the strong sector, for vertices of the form $gt\bar{c}$ or $gt\bar{u}$. In [1] the operators considered were:

$$\begin{aligned} \mathcal{O}_{tG} &= i\frac{\alpha_{it}^S}{\Lambda^2}(\bar{u}_R^i\lambda^a\gamma_\mu D_\nu t_R)G^{a\mu\nu} \\ \mathcal{O}_{tG\phi} &= \frac{\beta_{it}^S}{\Lambda^2}(\bar{q}_L^i\lambda^a\sigma^{\mu\nu}t_R)\phi G^{a\mu\nu}, \end{aligned} \quad (2.2)$$

where q_L and u_R are spinors, $\tilde{\phi}$ is the charge conjugate of the Higgs doublet, and $G_{\mu\nu}^a$ is the gluon tensor. There are other FCNC terms that come from these operators like for example $ggt\bar{u}$. However all other vertices are not relevant for this work. The constants α_{ij} and β_{ij} will play the role of coupling constants. Hence the dimension six Lagrangian terms for the gluon vertices are:

$$\mathcal{L} = \mathcal{O}_{tG} + \mathcal{O}_{tG\phi} + h.c., \quad (2.3)$$

where q stands a u or c quark. Finally, from this Lagrangian we extract the Feynman rules needed for the present work. They are shown in figure (2.1). The procedure for the electroweak sector is exactly the same [8]. In

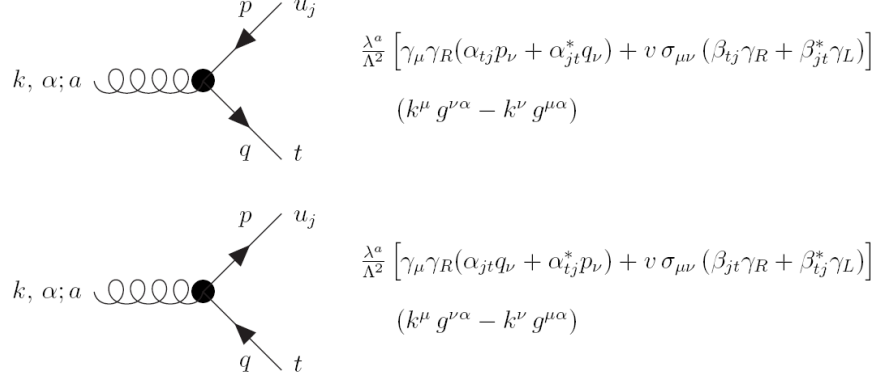


Figure 2.1: Feynman rules for anomalous $g\bar{u}_i t$ and $g\bar{t} u_i$.

equations (2.4)-(2.7) we present the operators for this sector.

$$\mathcal{O}_{tB} = i \frac{\alpha_{it}^B}{\Lambda^2} (\bar{u}_R^i \gamma_\mu D_\nu t_R) B^{\mu\nu}, \quad (2.4)$$

$$\mathcal{O}_{tB\phi} = \frac{\beta_{it}^B}{\Lambda^2} (\bar{q}_L^i \sigma^{\mu\nu} t_R) \tilde{\phi} B_{\mu\nu} \quad , \quad \mathcal{O}_{tW\phi} = \frac{\beta_{it}^W}{\Lambda^2} (\bar{q}_L^i \tau_I \sigma^{\mu\nu} t_R) \tilde{\phi} W_{\mu\nu}^I \quad (2.5)$$

$$\mathcal{O}_{\phi t} = \theta_{it} (\phi^\dagger D_\mu \phi) (\bar{u}_R^i \gamma^\mu t_R), \quad (2.6)$$

$$\mathcal{O}_{D_t} = \frac{\eta_{it}}{\Lambda^2} (\bar{q}_L^i D^\mu t_R) D_\mu \tilde{\phi} \quad , \quad \mathcal{O}_{\bar{D}_t} = \frac{\bar{\eta}_{it}}{\Lambda^2} (D^\mu \bar{q}_L^i t_R) D_\mu \tilde{\phi}, \quad (2.7)$$

where α_{it}^B , β_{it}^W , β_{it}^B , η_{it} , $\bar{\eta}_{it}$ and θ_{it} are complex dimensionless couplings; $B_{\mu\nu}$ is the $U(1)_Y$ field tensor and $W_{\mu\nu}^I$ is the $SU(2)_L$ field tensor. To isolate the contribution to the FCNC photon and Z interactions we define new effective couplings $\alpha^\gamma, \beta^\gamma$ and α^Z, β^Z . These are related to the initial couplings through the Weinberg angle θ_W by

$$\alpha^\gamma = \cos \theta_W \alpha^B \quad , \quad \alpha^Z = -\sin \theta_W \alpha^B \quad (2.8)$$

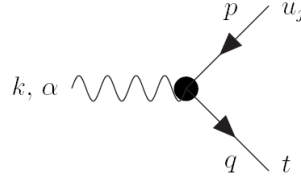
and

$$\begin{cases} \beta^\gamma = \sin \theta_W \beta^W + \cos \theta_W \beta^B \\ \beta^Z = \cos \theta_W \beta^W - \sin \theta_W \beta^B. \end{cases}$$

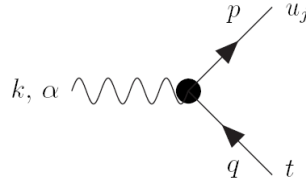
The Lagrangian that describes the electroweak interactions is

$$\mathcal{L} = \mathcal{O}_{tB} + \mathcal{O}_{tB\phi} + \mathcal{O}_{tW\phi} + \mathcal{O}_{\phi t} + \mathcal{O}_{D_t} + \mathcal{O}_{\bar{D}_t} + h.c. \quad (2.9)$$

In figures (2.2) and (2.3) the Feynman rules derived from this Lagrangian are shown.

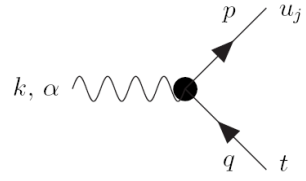


$$\frac{1}{\Lambda^2} \left[\gamma_\mu \gamma_R (\alpha_{tj}^{\gamma R} p_\nu + \alpha_{jt}^{\gamma R*} q_\nu) + v \sigma_{\mu\nu} (\beta_{tj}^{\gamma R} \gamma_R + \beta_{jt}^{\gamma L*} \gamma_L) \right] (k^\mu g^{\nu\alpha} - k^\nu g^{\mu\alpha})$$

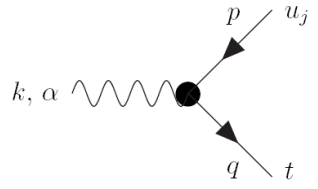


$$\frac{1}{\Lambda^2} \left[\gamma_\mu \gamma_R (\alpha_{jt}^{\gamma R} q_\nu + \alpha_{tj}^{\gamma R*} p_\nu) + v \sigma_{\mu\nu} (\beta_{jt}^{\gamma R} \gamma_R + \beta_{tj}^{\gamma L*} \gamma_L) \right] (k^\mu g^{\nu\alpha} - k^\nu g^{\mu\alpha})$$

Figure 2.2: Feynman rules for anomalous $\gamma \bar{u}_i t$ and $\gamma \bar{t} u_i$.



$$\frac{1}{\Lambda^2} \left[\gamma_\mu \gamma_R (\alpha_{jt}^{Z R} q_\nu + \alpha_{tj}^{Z R*} p_\nu) + v \sigma_{\mu\nu} (\beta_{jt}^{Z R} \gamma_R + \beta_{tj}^{Z L*} \gamma_L) \right] (k^\mu g^{\nu\alpha} - k^\nu g^{\mu\alpha}) + \frac{v}{\Lambda^2} [i \gamma_R (\eta_{jt} q_\alpha - \bar{\eta}_{jt} p_\alpha) + \theta v \gamma_\alpha \gamma_R]$$



$$\frac{1}{\Lambda^2} \left[\gamma_\mu \gamma_R (\alpha_{tj}^{Z R} p_\nu + \alpha_{jt}^{Z R*} q_\nu) + v \sigma_{\mu\nu} (\beta_{tj}^{Z R} \gamma_R + \beta_{jt}^{Z L*} \gamma_L) \right] (k^\mu g^{\nu\alpha} - k^\nu g^{\mu\alpha}) + \frac{v}{\Lambda^2} [i \gamma_L (\eta_{jt}^* q_\alpha - \bar{\eta}_{jt}^* p_\alpha) - \theta^* v \gamma_\alpha \gamma_R]$$

Figure 2.3: Feynman rules for anomalous $Z \bar{u}_i t$ and $Z \bar{t} u_i$.

Chapter 3

Single top Production

The production processes under consideration are $pp \rightarrow tq(qq \rightarrow tq)$ and $pp \rightarrow t\bar{q}(q\bar{q} \rightarrow t\bar{q})$, which means we are looking for final states with one top and one u or c quark. Additionally we restrict the calculation to a single flavour violation in the production process, which means we will have only one FCNC vertex. The general form of the diagrams for $qq \rightarrow tq$ and $q\bar{q} \rightarrow t\bar{q}$ are represented in figures (3.1) - (3.4). The set of all possible processes under these constraints are summarised in table 3.1. For process 1 we must consider the t and u channels of figures (3.1) and (3.2) and for process 3 the t and s channels of figures (3.3) and (3.4). These are the only processes with two channels. For processes 2 and 4 to 8 there is only one allowed channel: a t channel for processes 2, 5, 7 and 8 and an s channel for processes 4 and 6. Note that table 3.1 presents only the processes where the anomalous couplings under study involve the u and t quarks. For the full calculation the anomalous coupling between c and t quarks was also considered. Since the calculation for the c coupling follow the rule of u coupling, I will only present the u coupling processes for simplicity. In addition, for processes 6 to 8, the d quark, represents a d, s or b quark. In figure 3.5 we can see the

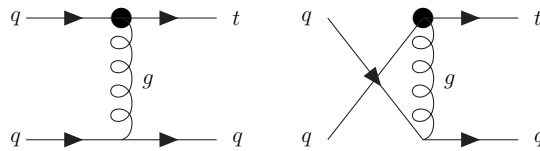


Figure 3.1: Feynman diagrams of $qq \rightarrow tq$ process for the strong sector.

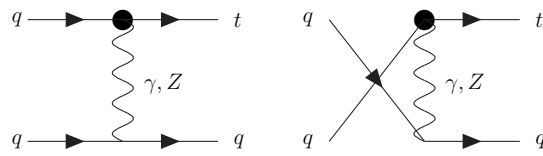


Figure 3.2: Feynman diagrams of $qq \rightarrow tq$ process for the electroweak sector.

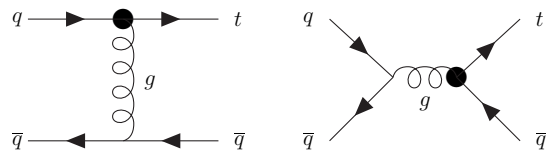


Figure 3.3: Feynman diagrams of $q\bar{q} \rightarrow t\bar{q}$ process for the strong sector.

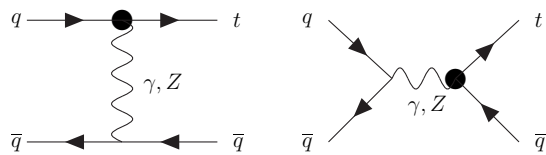


Figure 3.4: Feynman diagrams of $q\bar{q} \rightarrow t\bar{q}$ process for the electroweak sector.

Single top channel	Process number
$uu \rightarrow tu$	1
$uc \rightarrow tc$	2
$u\bar{u} \rightarrow t\bar{u}$	3
$u\bar{u} \rightarrow t\bar{c}$	4
$u\bar{c} \rightarrow t\bar{c}$	5
$d\bar{d} \rightarrow t\bar{u}$	6
$ud \rightarrow td$	7
$u\bar{d} \rightarrow t\bar{d}$	8

Table 3.1: FCNC single-top production processes considered.

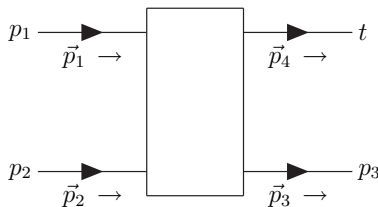


Figure 3.5: Momentum convention.

labels for the particle's momentum defined for this calculation. The usual definition of the Mandelstam variables: $s = (p_1 + p_2)^2$, $t = (p_4 - p_1)^2$ and $u = (p_4 - p_2)^2$ was used. The kinematical conditions for all calculations are defined in table 3.2. Except for the top, all the quark masses were set to zero.

Finally we will separate the calculations in two parts. The first part will consider processes 1 to 5 and the second part the process 6 to 8. Although there is no tree level SM equivalent process that competes with the first five processes, this is not the case for processes 6 to 8. For the reasons explained, the first anomalous contributions for the processes 6 to 8 is of order $\frac{1}{\Lambda^2}$. For simplicity I will describe in more detail the calculation associated to process 1, since for processes 2 to 5 the procedure is similar.

$p_1 \cdot p_1 = m_g^2 = 0$
$p_2 \cdot p_2 = m_g^2 = 0$
$p_3 \cdot p_3 = m_g^2 = 0$
$p_4 \cdot p_4 = m_q^2 = m_t^2$
$p_1 \cdot p_2 = \frac{s}{2}$
$p_1 \cdot p_3 = -\frac{u}{2}$
$p_1 \cdot p_4 = \frac{s+u}{2}$
$p_2 \cdot p_3 = -\frac{t}{2}$
$p_2 \cdot p_4 = \frac{s+t}{2}$
$p_3 \cdot p_4 = -\frac{t+u}{2}$
$s + t + u = m_t^2$
$p_1 + p_2 = p_3 + p_4$

Table 3.2: Kinematics constrains.

3.1 Process 1

For process 1 we have $uu \rightarrow tu$ (u coupling). We define the functions $V_i(p, q, k)$ and $\bar{V}_i(p, q, k) = \gamma^0 V_i^\dagger(p, q, k) \gamma^0$, with $i = g, \gamma, Z$, which are the FCNC vertices defined in equations (2.1)-(2.3) without the Gell-Mann matrices (we will work them explicitly). The SM Feynman rules used can be seen in the appendix. For this process we have two identical particles which result in one t channel and one u channel contribution to the process. The transition amplitudes for the gluon, photon and Z to this process are, respectively:

$$iT_g^t = [\bar{u}_t^i V_g^\mu(p_1, p_4, p_4 - p_1) 2t_{ij}^a u_1^j] \left(\frac{-ig_{\mu\nu}}{t} \right) [\bar{u}_3^k i g_3 t_{kl}^a \gamma^\nu u_2^l] \quad (3.1)$$

$$iT_g^u = -[\bar{u}_t^i V_g^\mu(p_2, p_4, p_4 - p_2) 2t_{ij}^a u_2^j] \left(\frac{-ig_{\mu\nu}}{u} \right) [\bar{u}_3^k i g_3 t_{kl}^a \gamma^\nu u_1^l] \quad (3.2)$$

$$iT_\gamma^t = [\bar{u}_t^i V_\gamma^\mu(p_1, p_4, p_4 - p_1) \delta_{ij} u_1^j] \left(\frac{-ig_{\mu\nu}}{t} \right) [\bar{u}_3^k i e Q_u \gamma^\nu \delta_{kl} u_2^l] \quad (3.3)$$

$$iT_\gamma^u = -[\bar{u}_t^i V_\gamma^\mu(p_2, p_4, p_4 - p_2) \delta_{ij} u_2^j] \left(\frac{-ig_{\mu\nu}}{u} \right) [\bar{u}_3^k i e Q_u \gamma^\nu \delta_{kl} u_1^l] \quad (3.4)$$

$$iT_Z^t = [\bar{u}_t^i V_Z^\mu(p_1, p_4, p_4 - p_1) \delta_{ij} u_1^j] \left(\frac{-i}{t - m_z^2} \right) \left(g_{\mu\nu} - \frac{k_\mu k_\nu}{m_z^2} \right) [\bar{u}_3^k \frac{i e}{\sin(2\theta_w)} \gamma_\nu [T_3 - 2Q_u^2 \sin^2(\theta_w) - T_3 \gamma_5] \delta_{kl} u_2^l] \quad (3.5)$$

$$\begin{aligned}
iT_Z^u &= -[\bar{u}_t^i V_Z^\mu(p_2, p_4, p_4 - p_2) \delta_{ij} u_2^j] \left(\frac{-i}{u - m_z^2} \right) (g_{\mu\nu} - \frac{k_\mu k_\nu}{m_z^2}) \\
&\quad [\bar{u}_3^k \frac{ie}{\sin(2\theta_w)} \gamma_\nu [T_3 - 2Q_u^2 \sin^2(\theta_w) - T_3 \gamma_5] \delta_{kl} u_1^l] \quad (3.6)
\end{aligned}$$

where u_m^i is the spinor, $m = t, 1, 2, 3$ is the index that defines the particle, $2t_{ij}^a$ correspond to the Gell-Mann matrices where $a = 1, \dots, 8$, the indices i, j, k, l define the particle's colour, g_3 is the strong coupling constant, Q_u is the u quark charge and $T_3 = \frac{1}{2}$ in this case. Now we want to calculate the average of the total amplitude squared:

$$iT_{total} = iT_g^t + iT_g^u + iT_\gamma^t + iT_\gamma^u + iT_Z^t + iT_Z^u. \quad (3.7)$$

This results in a total of $6 \times 6 = 36$ terms. From these 36 terms 8 are be zero for the reasons to be explained bellow. For simplicity we will separate the spin and colour averages calculations for each boson channel, and for the respective interferences.

Gluon

The averages for the gluon channel are written in equations 3.8-3.11. In all four contributions we have the factor $\frac{1}{4 \times 9}$ and the usual Gell-Mann traces from the averaging over the initial colour states

$$\begin{aligned}
\langle T_g^t (T_g^t)^\dagger \rangle &= \frac{1}{4 \times 9} \frac{4g_3^2}{t^2} Tr[t^a t^b] Tr[t^a t^b] \\
&\quad \times Tr[V_g^\alpha(p_1, p_4, p_4 - p_1) \cdot \not{p}_1 \cdot \bar{V}_g^\beta(p_1, p_4, p_4 - p_1) \cdot (\not{p}_4 + m_t)] \\
&\quad \times Tr[\gamma_\alpha \cdot \not{p}_2 \cdot \gamma_\beta \cdot \not{p}_3] \quad (3.8)
\end{aligned}$$

$$\begin{aligned}
\langle T_g^u (T_g^u)^\dagger \rangle &= \frac{1}{4 \times 9} \frac{4g_3^2}{u^2} Tr[t^a t^b] Tr[t^a t^b] \\
&\quad \times Tr[V_g^\alpha(p_2, p_4, p_4 - p_2) \cdot \not{p}_2 \cdot \bar{V}_g^\beta(p_2, p_4, p_4 - p_2) \cdot (\not{p}_4 + m_t)] \\
&\quad \times Tr[\gamma_\alpha \cdot \not{p}_1 \cdot \gamma_\beta \cdot \not{p}_3] \quad (3.9)
\end{aligned}$$

$$\begin{aligned}
\langle T_g^t (T_g^u)^\dagger \rangle &= \frac{1}{4 \times 9} \frac{-4g_3^2}{tu} Tr[t^a t^b t^a t^b] \\
&\quad Tr[\bar{V}_g^\alpha(p_2, p_4, p_4 - p_2) \cdot (\not{p}_4 + m_t) \cdot V_g^\beta(p_1, p_4, p_4 - p_1) \cdot \\
&\quad \not{p}_1 \cdot \gamma_\alpha \cdot \not{p}_3 \cdot \gamma_\beta \cdot \not{p}_2] \quad (3.10)
\end{aligned}$$

$$\begin{aligned}
\langle T_g^u(T_g^t)^\dagger \rangle &= \frac{1}{4 \times 9} \frac{-4g_3^2}{tu} Tr[t^a t^b t^a t^b] \\
&\quad Tr[\bar{V}_g^\alpha(p_1, p_4, p_4 - p_1) \cdot (\not{p}_4 + m_t) \cdot V_g^\beta(p_2, p_4, p_4 - p_2) \cdot \\
&\quad \not{p}_2 \cdot \gamma_\alpha \cdot \not{p}_3 \cdot \gamma_\beta \cdot \not{p}_1]. \tag{3.11}
\end{aligned}$$

Photon

The calculation for the photon channel is similar to the one for the gluon channel. We will discuss briefly how to account for the colour factor. Although no colour exchange takes place in a photon vertex, we have to average over the initial quarks colour. There are two different cases: the interference between same channel diagrams and the one between different channels. In the first one the colour indices contraction will be divided in two delta matrix traces (equations (3.12) and (3.13)) which is equal to 9. In the second one there is a crossing between fermionic lines that results in only one delta matrix trace (equations (3.14) and (3.15)) which is equal to 3.

$$\begin{aligned}
\langle T_\gamma^t(T_\gamma^t)^\dagger \rangle &= \frac{1}{4 \times 9} \left(\frac{eQ_u}{t}\right)^2 Tr[\delta] Tr[\delta] \\
&\quad \times Tr[V_\gamma^\alpha(p_1, p_4, p_4 - p_1) \cdot \not{p}_1 \cdot \bar{V}_\gamma^\beta(p_1, p_4, p_4 - p_1) \cdot (\not{p}_4 + m_t)] \\
&\quad \times Tr[\gamma_\alpha \cdot \not{p}_2 \cdot \gamma_\beta \cdot \not{p}_3] \tag{3.12}
\end{aligned}$$

$$\begin{aligned}
\langle T_\gamma^u(T_\gamma^u)^\dagger \rangle &= \frac{1}{4 \times 9} \left(\frac{eQ_u}{u}\right)^2 Tr[\delta] Tr[\delta] \\
&\quad \times Tr[V_\gamma^\alpha(p_2, p_4, p_4 - p_2) \cdot \not{p}_2 \cdot \bar{V}_\gamma^\beta(p_2, p_4, p_4 - p_2) \cdot (\not{p}_4 + m_t)] \\
&\quad \times Tr[\gamma_\alpha \cdot \not{p}_1 \cdot \gamma_\beta \cdot \not{p}_3] \tag{3.13}
\end{aligned}$$

$$\begin{aligned}
\langle T_\gamma^t(T_\gamma^u)^\dagger \rangle &= \frac{1}{4 \times 9} \frac{-(eQ_u)^2}{tu} Tr[\delta] \\
&\quad Tr[V_\gamma^\alpha(p_1, p_4, p_4 - p_1) \cdot \not{p}_1 \cdot \gamma_\beta \cdot \not{p}_3 \cdot \gamma_\alpha \cdot \not{p}_2 \cdot \bar{V}_\gamma^\beta(p_2, p_4, p_4 - p_2) \cdot \\
&\quad (\not{p}_4 + m_t)] \tag{3.14}
\end{aligned}$$

$$\begin{aligned}
\langle T_\gamma^u(T_\gamma^t)^\dagger \rangle &= \frac{1}{4 \times 9} \frac{-(eQ_u)^2}{tu} Tr[\delta] \\
&\quad Tr[V_\gamma^\alpha(p_2, p_4, p_4 - p_2) \cdot \not{p}_2 \cdot \gamma_\beta \cdot \not{p}_3 \cdot \gamma_\alpha \cdot \not{p}_1 \cdot \bar{V}_\gamma^\beta(p_1, p_4, p_4 - p_1) \cdot \\
&\quad (\not{p}_4 + m_t)]. \tag{3.15}
\end{aligned}$$

To visualise the calculation of the colour factors in the electroweak sector, imagine one simple model where we have two colours. From figures (3.6)-(3.9) we can see the Feynman diagrams for each possible colour combination in this model. The superscripts indices mean yellow and blue. We can see that we would have 4 terms for the transition amplitude in each channel. This means that if we would like to know the average of the transition amplitude of the t channel, for example, we would have to sum these four amplitudes and divide by the number of possible initial combination, which in this case is $2 \times 2 = 4$. In this way the colour factor would be one in the t and u channels. For the interference this is not true. Since with a u channel the final particles are inverted with respect to the t channel, there are only two terms that contribute to the interferences. We can see this for figures (3.7) and (3.8). The final state of both channels for these combinations is not coincident and therefore it results a in null transition amplitude. This is not the case for figures (3.6) and (3.9), where the initial and final states are equal. Therefore, for the total interference contribution we would have a $\frac{2}{4}$ factor, equivalente to the $\frac{2}{9}$ factor resulted obtained in our actual calculation.

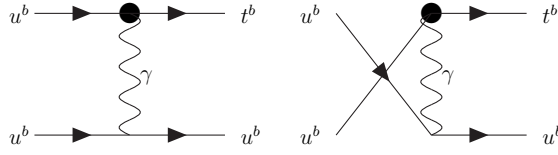


Figure 3.6: Feynman diagrams for $u^b u^b \rightarrow t^b u^b$ process.

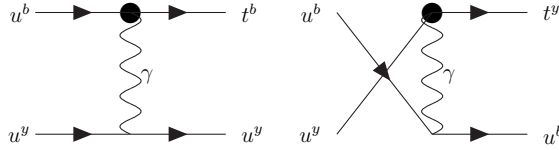


Figure 3.7: Feynman diagrams for $u^b u^y \rightarrow t^b u^y$ (t channel) and $u^b u^y \rightarrow t^y u^b$ (u channel) processes.

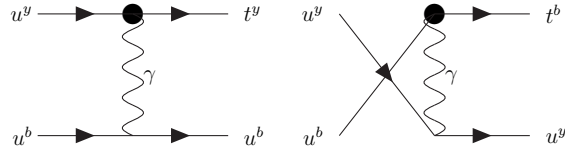


Figure 3.8: Feynman diagrams for $u^y u^b \rightarrow t^y u^b$ (t channel) and $u^y u^b \rightarrow t^b u^y$ (u channel) processes.

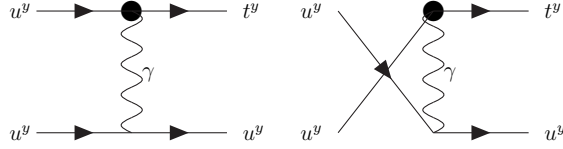


Figure 3.9: Feynman diagrams for $u^y u^y \rightarrow t^y u^y$ process.

Z

For the Z channel we first define the functions:

$$\Gamma(k, Q)_\mu = \left(g_{\mu\nu} - \frac{k_\mu k_\nu}{m_z^2}\right) \gamma^\nu (T_3 - 2Q^2 s_w^2 - T_3 \gamma^5) \quad (3.16)$$

$$\bar{\Gamma}(k, Q)_\mu = \left(g_{\mu\nu} - \frac{k_\mu k_\nu}{m_z^2}\right) (T_3 - 2Q^2 s_w^2 + T_3 \gamma^5) \gamma^\nu. \quad (3.17)$$

Apart from the vertices and the propagator, the calculations for this channel are the same as for the photon channel. Likewise, the colour factors will be the same since there is no difference in colour counting for this channel. Therefore the average of the square of transition amplitudes are:

$$\begin{aligned} \langle T_z^t (T_z^t)^\dagger \rangle &= \frac{1}{4 \times 9} \frac{e^2}{4s_w^2 c_w^2 (t - m_z^2)^2} \text{Tr}[\delta] \text{Tr}[\delta] \\ &\quad \times \text{Tr}[V_Z^\alpha(p_1, p_4, p_4 - p_1) \cdot \not{p}_1 \cdot \bar{V}_Z^\beta(p_1, p_4, p_4 - p_1) \cdot (\not{p}_4 + m_t)] \\ &\quad \times \text{Tr}[\Gamma_\alpha(p_4 - p_1, Q_u) \cdot \not{p}_2 \cdot \bar{\Gamma}_\beta(p_4 - p_1, Q_u) \cdot \not{p}_3] \quad (3.18) \end{aligned}$$

$$\begin{aligned}
\langle T_z^u(T_z^u)^\dagger \rangle &= \frac{1}{4 \times 9} \frac{e^2}{4s_w^2 c_w^2 (u - m_z^2)^2} Tr[\delta] Tr[\delta] \\
&\times Tr[V_Z^\alpha(p_2, p_4, p_4 - p_2) \cdot \not{p}_2 \cdot \bar{V}_Z^\beta(p_2, p_4, p_4 - p_2) \cdot (\not{p}_4 + m_t)] \\
&\times Tr[\Gamma_\alpha(p_4 - p_2, Q_u) \cdot \not{p}_1 \cdot \bar{\Gamma}_\beta(p_4 - p_2, Q_u) \cdot \not{p}_3] \quad (3.19)
\end{aligned}$$

$$\begin{aligned}
\langle T_z^t(T_z^t)^\dagger \rangle &= \frac{1}{4 \times 9} \frac{-e^2}{4s_w c_w (t - m_z^2)(u - m_z^2)} Tr[\delta] \\
&\times Tr[V_Z^\alpha(p_1, p_4, p_4 - p_1) \cdot \not{p}_1 \cdot \bar{\Gamma}_\beta(p_4 - p_2, Q_u) \cdot \not{p}_3 \cdot \Gamma_\alpha(p_4 - p_1, Q_u) \cdot \\
&\times \not{p}_2 \cdot \bar{V}_z^\beta(p_2, p_4, p_4 - p_2) \cdot (\not{p}_4 + m_t)] \quad (3.20)
\end{aligned}$$

$$\begin{aligned}
\langle T_z^u(T_z^t)^\dagger \rangle &= \frac{1}{4 \times 9} \frac{-e^2}{4s_w c_w (t - m_z^2)(u - m_z^2)} Tr[\delta] \\
&\times Tr[V_Z^\alpha(p_2, p_4, p_4 - p_2) \cdot \not{p}_2 \cdot \bar{\Gamma}_\beta(p_4 - p_1, Q_u) \cdot \not{p}_3 \cdot \Gamma_\alpha(p_4 - p_2, Q_u) \cdot \\
&\times \not{p}_1 \cdot \bar{V}_z^\beta(p_1, p_4, p_4 - p_1) \cdot (\not{p}_4 + m_t)]. \quad (3.21)
\end{aligned}$$

Gluon and Photon interference

For all the interferences the calculations are equivalent to the ones performed before. For the same channels, the interference between the strong and electroweak sector vanishes. This is the case for the process 2,4 and 5. For these cases we have two traces of the form $Tr[t^a]$, which are null. For the photon and Z sectors this does not happen and the colour term is equal to unity. For two different channels in the strong-electroweak sector we have the trace $Tr[t^a t^a] = 4$. Finally for the photon and Z sectors we have again the colour factor $\frac{1}{3}$,

$$\begin{aligned}
\langle T_g^t(T_\gamma^u)^\dagger \rangle &= \frac{1}{4 \times 9} \frac{-2eg_3 Q_u}{tu} Tr[t^a t^a] \\
&\times Tr[(\not{p}_4 + m_t) \cdot V_g^\alpha(p_1, p_4, p_4 - p_1) \cdot \not{p}_1 \cdot \gamma_\beta \cdot \not{p}_3 \cdot \gamma_\alpha \cdot \not{p}_2 \cdot \\
&\bar{V}_\gamma^\beta(p_2, p_4, p_4 - p_2)] \quad (3.22)
\end{aligned}$$

$$\begin{aligned}
\langle T_\gamma^u(T_g^t)^\dagger \rangle &= \frac{1}{4 \times 9} \frac{-2eg_3 Q_u}{tu} Tr[t^a t^a] \\
&\times Tr[(\not{p}_4 + m_t) \cdot V_\gamma^\beta(p_2, p_4, p_4 - p_2) \cdot \not{p}_2 \cdot \gamma_\alpha \cdot \not{p}_3 \cdot \gamma_\beta \cdot \not{p}_1 \cdot \\
&\bar{V}_g^\alpha(p_1, p_4, p_4 - p_1)] \quad (3.23)
\end{aligned}$$

$$\begin{aligned}
\langle T_g^u(T_\gamma^t)^\dagger \rangle &= \frac{1}{4 \times 9} \frac{-2eg_3 Q_u}{tu} \text{Tr}[t^a t^a] \\
&\times \text{Tr}[(\not{p}_4 + m_t) \cdot V_g^\beta(p_2, p_4, p_4 - p_2) \cdot \not{p}_2 \cdot \gamma_\alpha \cdot \not{p}_3 \cdot \gamma_\beta \cdot \not{p}_1 \cdot \\
&\bar{V}_\gamma^\alpha(p_1, p_4, p_4 - p_1)] \quad (3.24)
\end{aligned}$$

$$\begin{aligned}
\langle T_\gamma^t(T_g^u)^\dagger \rangle &= \frac{1}{4 \times 9} \frac{-2eg_3 Q_u}{tu} \text{Tr}[t^a t^a] \\
&\times \text{Tr}[(\not{p}_4 + m_t) \cdot V_\gamma^\alpha(p_1, p_4, p_4 - p_1) \cdot \not{p}_1 \cdot \gamma_\beta \cdot \not{p}_3 \cdot \gamma_\alpha \cdot \not{p}_2 \cdot \\
&\bar{V}_g^\alpha(p_2, p_4, p_4 - p_2)] \quad (3.25)
\end{aligned}$$

$$\langle T_g^t(T_\gamma^t)^\dagger \rangle = \langle T_\gamma^t(T_g^t)^\dagger \rangle = \langle T_g^u(T_\gamma^u)^\dagger \rangle = \langle T_\gamma^u(T_g^u)^\dagger \rangle = 0. \quad (3.26)$$

Gluon and Z interference

$$\begin{aligned}
\langle T_g^t(T_z^u)^\dagger \rangle &= \frac{1}{4 \times 9} \frac{-eg_3}{s_w c_w t(u - m_z^2)} \text{Tr}[t^a t^a] \\
&\times \text{Tr}[(\not{p}_4 + m_t) \cdot V_g^\alpha(p_1, p_4, p_4 - p_1) \cdot \not{p}_1 \cdot \bar{\Gamma}_\beta(p_4 - p_2, Q_u) \cdot \not{p}_3 \cdot \gamma_\alpha \cdot \not{p}_2 \cdot \\
&\bar{V}_z^\beta(p_2, p_4, p_4 - p_2)] \quad (3.27)
\end{aligned}$$

$$\begin{aligned}
\langle T_z^u(T_g^t)^\dagger \rangle &= \frac{1}{4 \times 9} \frac{-eg_3}{s_w c_w t(u - m_z^2)} \text{Tr}[t^a t^a] \\
&\times \text{Tr}[(\not{p}_4 + m_t) \cdot V_z^\beta(p_2, p_4, p_4 - p_2, Q_u) \cdot \not{p}_2 \cdot \gamma_\alpha \cdot \not{p}_3 \cdot \Gamma_\beta(p_4 - p_2, Q_u) \cdot \not{p}_1 \cdot \\
&\bar{V}_g^\alpha(p_1, p_4, p_4 - p_1)] \quad (3.28)
\end{aligned}$$

$$\begin{aligned}
\langle T_g^u(T_z^t)^\dagger \rangle &= \frac{1}{4 \times 9} \frac{-eg_3}{s_w c_w u(t - m_z^2)} \text{Tr}[t^a t^a] \\
&\times \text{Tr}[(\not{p}_4 + m_t) \cdot V_g^\beta(p_2, p_4, p_4 - p_2) \cdot \not{p}_2 \cdot \bar{\Gamma}_\alpha(p_4 - p_1, Q_u) \cdot \not{p}_3 \cdot \gamma_\beta \cdot \not{p}_1 \cdot \\
&\bar{V}_z^\alpha(p_1, p_4, p_4 - p_1)] \quad (3.29)
\end{aligned}$$

$$\begin{aligned}
\langle T_z^t(T_g^u)^\dagger \rangle &= \frac{1}{4 \times 9} \frac{-eg_3}{s_w c_w u(t - m_z^2)} \text{Tr}[t^a t^a] \\
&\times \text{Tr}[(\not{p}_4 + m_t) \cdot V_z^\alpha(p_1, p_4, p_4 - p_1) \cdot \not{p}_1 \cdot \gamma_\beta \cdot \not{p}_3 \cdot \Gamma_\alpha(p_4 - p_1, Q_u) \cdot \not{p}_2 \cdot \\
&\bar{V}_g^\beta(p_2, p_4, p_4 - p_2)] \quad (3.30)
\end{aligned}$$

$$\langle T_g^t(T_z^t)^\dagger \rangle = \langle T_z^t(T_g^t)^\dagger \rangle = \langle T_g^u(T_z^u)^\dagger \rangle = \langle T_z^u(T_g^u)^\dagger \rangle = 0. \quad (3.31)$$

Photon and Z interference

$$\begin{aligned}
\langle T_\gamma^t(T_z^t)^\dagger \rangle &= \frac{1}{4 \times 9} \frac{e^2 Q_u}{2t s_w c_w (t - m_z^2)} \text{Tr}[\delta] \text{Tr}[\delta] \\
&\times \text{Tr}[(\not{p}_4 + m_t) \cdot V_\gamma^\alpha(p_1, p_4, p_4 - p_1) \cdot \not{p}_1 \cdot \bar{V}_z^\beta(p_1, p_4, p_4 - p_1)] \\
&\times \text{Tr}[\not{p}_3 \cdot \gamma_\alpha \cdot \not{p}_2 \cdot \bar{\Gamma}_\beta(p_4 - p_1, Q_u)] \tag{3.32}
\end{aligned}$$

$$\begin{aligned}
\langle T_\gamma^t(T_z^u)^\dagger \rangle &= \frac{1}{4 \times 9} \frac{-e^2 Q_u}{2t s_w c_w (u - m_z^2)} \text{Tr}[\delta] \\
&\times \text{Tr}[(\not{p}_4 + m_t) \cdot V_\gamma^\alpha(p_1, p_4, p_4 - p_1) \cdot \not{p}_1 \cdot \bar{\Gamma}_\beta(p_4 - p_2, Q_u) \cdot \not{p}_3 \cdot \gamma_\alpha \cdot \not{p}_2 \cdot \\
&\bar{V}_z^\beta(p_2, p_4, p_4 - p_2)] \tag{3.33}
\end{aligned}$$

$$\begin{aligned}
\langle T_\gamma^u(T_z^t)^\dagger \rangle &= \frac{1}{4 \times 9} \frac{-e^2 Q_u}{2u s_w c_w (t - m_z^2)} \text{Tr}[\delta] \\
&\times \text{Tr}[(\not{p}_4 + m_t) \cdot V_\gamma^\alpha(p_2, p_4, p_4 - p_2) \cdot \not{p}_2 \cdot \bar{\Gamma}_\beta(p_4 - p_1, Q_u) \cdot \not{p}_3 \cdot \gamma_\alpha \cdot \not{p}_1 \cdot \\
&\bar{V}_z^\beta(p_1, p_4, p_4 - p_1)] \tag{3.34}
\end{aligned}$$

$$\begin{aligned}
\langle T_\gamma^u(T_z^u)^\dagger \rangle &= \frac{1}{4 \times 9} \frac{e^2 Q_u}{2u s_w c_w (u - m_z^2)} \text{Tr}[\delta] \text{Tr}[\delta] \\
&\times \text{Tr}[(\not{p}_4 + m_t) \cdot V_\gamma^\alpha(p_2, p_4, p_4 - p_2) \cdot \not{p}_2 \cdot \bar{V}_z^\beta(p_2, p_4, p_4 - p_2)] \\
&\times \text{Tr}[\not{p}_3 \cdot \gamma_\alpha \cdot \not{p}_1 \cdot \bar{\Gamma}_\beta(p_4 - p_2, Q_u)] \tag{3.35}
\end{aligned}$$

$$\begin{aligned}
\langle T_z^t(T_\gamma^t)^\dagger \rangle &= \frac{1}{4 \times 9} \frac{e^2 Q_u}{2t s_w c_w (t - m_z^2)} \text{Tr}[\delta] \text{Tr}[\delta] \\
&\times \text{Tr}[(\not{p}_4 + m_t) \cdot V_z^\beta(p_1, p_4, p_4 - p_1) \cdot \not{p}_1 \cdot \bar{V}_\gamma^\alpha(p_1, p_4, p_4 - p_1)] \\
&\times \text{Tr}[\not{p}_3 \Gamma_\beta(p_4 - p_1, Q_u) \cdot \not{p}_2 \cdot \gamma_\alpha] \tag{3.36}
\end{aligned}$$

$$\begin{aligned}
\langle T_z^t(T_\gamma^u)^\dagger \rangle &= \frac{1}{4 \times 9} \frac{-e^2 Q_u}{2u s_w c_w (t - m_z^2)} \text{Tr}[\delta] \\
&\times \text{Tr}[(\not{p}_4 + m_t) \cdot V_z^\beta(p_1, p_4, p_4 - p_1) \cdot \not{p}_1 \cdot \gamma_\alpha \cdot \not{p}_3 \cdot \Gamma_\beta(p_4 - p_1, Q_u) \cdot \not{p}_2 \cdot \\
&\bar{V}_\gamma^\alpha(p_2, p_4, p_4 - p_2)] \tag{3.37}
\end{aligned}$$

$$\begin{aligned}
\langle T_z^u(T_\gamma^t)^\dagger \rangle &= \frac{1}{4 \times 9} \frac{-e^2 Q_u}{2t s_w c_w (u - m_z^2)} \text{Tr}[\delta] \\
&\times \text{Tr}[(\not{p}_4 + m_t) \cdot V_z^\beta(p_2, p_4, p_4 - p_2) \cdot \not{p}_2 \cdot \gamma_\alpha \cdot \not{p}_3 \cdot \Gamma_\beta(p_4 - p_2, Q_u) \cdot \not{p}_1 \cdot \\
&\bar{V}_\gamma^\alpha(p_1, p_4, p_4 - p_1)] \tag{3.38}
\end{aligned}$$

$$\begin{aligned}
\langle T_z^u(T_\gamma^u)^\dagger \rangle &= \frac{1}{4 \times 9} \frac{e^2 Q_u}{2u s_w c_w (u - m_z^2)} Tr[\delta] Tr[\delta] \\
&\times Tr[(\not{p}_4 + m_t) \cdot V_z^\beta(p_2, p_4, p_4 - p_2) \cdot \not{p}_2 \cdot \bar{V}_\gamma^\alpha(p_2, p_4, p_4 - p_2)] \\
&\times Tr[\not{p}_3 \cdot \Gamma_\beta(p_4 - p_2, Q_u) \cdot \not{p}_1 \cdot \gamma_\alpha]. \tag{3.39}
\end{aligned}$$

3.1.1 Results

Apart from a common factor, the previous results are the differential cross section for the production process under consideration. Since the expressions are very long we will not show them here. For processes 1 and 3, they are summarised in 66 terms. As we saw earlier, the interferences between the gluon and electroweak channels for the processes 2, 4 and 5 are zero. Therefore for these processes we have a total of 45 terms. All terms are associated to the anomalous couplings constants from the FCNC vertices. Apart from the 21 null terms for the processes 2, 4 and 5, the set of constants is the same for all the processes. In tables 3.3 and 3.4, the set of anomalous constants associated to the 66 terms are shown. The convention adopted to label the terms is: F for the gluon channel, G for the photon channel, H for the Z channel, and FG, FH and GH for the interferences of the corresponding channels.

Gluon	Photon	Z	Z
F1 $\alpha_{ut}^g (\alpha_{ut}^g)^*$	G1 $\alpha_{ut}^\gamma (\alpha_{ut}^\gamma)^*$	H1 $\alpha_{ut}^Z (\alpha_{ut}^Z)^*$	H8 $Re[\alpha_{tu}^Z \alpha_{ut}^Z]$
F2 $\alpha_{tu}^g (\alpha_{tu}^g)^*$	G2 $\alpha_{tu}^\gamma (\alpha_{tu}^\gamma)^*$	H2 $\alpha_{tu}^Z (\alpha_{tu}^Z)^*$	H9 $Im[\alpha_{ut}^Z \beta_{tu}^Z]$
F3 $\beta_{ut}^g (\beta_{ut}^g)^*$	G3 $\beta_{ut}^\gamma (\beta_{ut}^\gamma)^*$	H3 $\beta_{ut}^Z (\beta_{ut}^Z)^*$	H10 $Re[\alpha_{ut}^Z \theta^*]$
F4 $\beta_{tu}^g (\beta_{tu}^g)^*$	G4 $\beta_{tu}^\gamma (\beta_{tu}^\gamma)^*$	H4 $\beta_{tu}^Z (\beta_{tu}^Z)^*$	H11 $Im[\alpha_{tu}^Z (\beta_{tu}^Z)^*]$
F5 $Re[\alpha_{tu}^g \alpha_{ut}^g]$	G5 $Re[\alpha_{tu}^\gamma (\alpha_{ut}^\gamma)]$	H5 $\eta\eta^*$	H12 $Re[\theta \alpha_{tu}^Z]$
F6 $Im[\alpha_{ut}^g \beta_{tu}^g]$	G6 $Im[\alpha_{ut}^\gamma (\beta_{tu}^\gamma)]$	H6 $\bar{\eta}\bar{\eta}^*$	H13 $Re[\beta_{ut}^Z \bar{\eta}^*]$
F7 $Im[\alpha_{tu}^g (\beta_{tu}^g)^*]$	G7 $Im[\alpha_{tu}^\gamma (\beta_{tu}^\gamma)^*]$	H7 $\theta\theta^*$	H14 $Re[\beta_{ut}^Z \bar{\eta}^*]$
			H15 $Im[\theta \beta_{tu}^Z]$
			H16 $Re[\eta\bar{\eta}^*]$

Table 3.3: Anomalous constants from the Gluon, Photon, and Z channel results.

Equation (3.40) shows a simplified representation of the average of the total transition amplitude squared for process 1. As an example, the term

Gluon-Photon	Gluon-Z	Photon-Z
FG1 $Re[\alpha_{ut}^g(\alpha_{ut}^\gamma)^*]$	FH1 $Re[\alpha_{ut}^g(\alpha_{ut}^Z)^*]$	GH1 $Re[\alpha_{ut}^\gamma(\alpha_{ut}^Z)^*]$
FG2 $Re[\alpha_{tu}^\gamma\alpha_{ut}^g]$	FH2 $Re[\alpha_{ut}^g\alpha_{tu}^Z]$	GH2 $Re[\alpha_{ut}^\gamma\alpha_{tu}^Z]$
FG3 $Im[\alpha_{ut}^g\beta_{tu}^\gamma]$	FH3 $Im[\alpha_{ut}^g\beta_{tu}^Z]$	GH3 $Im[\alpha_{ut}^\gamma\beta_{tu}^Z]$
FG4 $Re[\alpha_{ut}^\gamma\alpha_{tu}^g]$	FH4 $Re[\alpha_{ut}^g\theta^*]$	GH4 $Re[\alpha_{ut}^\gamma\theta^*]$
FG5 $Re[\alpha_{tu}^g(\alpha_{tu}^\gamma)^*]$	FH5 $Re[\alpha_{tu}^g\alpha_{tu}^Z]$	GH5 $Re[\alpha_{tu}^\gamma\alpha_{tu}^Z]$
FG6 $Re[\beta_{ut}^g(\beta_{ut}^\gamma)^*]$	FH6 $Re[\alpha_{tu}^g(\alpha_{tu}^Z)^*]$	GH6 $Re[\alpha_{tu}^\gamma(\alpha_{tu}^Z)^*]$
FG7 $Im[\alpha_{ut}^\gamma\beta_{tu}^g]$	FH7 $Re[\theta\alpha_{tu}^g]$	GH7 $Im[\alpha_{tu}^\gamma(\beta_{tu}^Z)^*]$
FG8 $Re[\alpha_{tu}^g(\beta_{tu}^\gamma)^*]$	FH8 $Re[\beta_{ut}^g(\beta_{ut}^Z)^*]$	GH8 $Re[\theta\alpha_{tu}^\gamma]$
	FH9 $Re[\beta_{ut}^g\eta^*]$	GH9 $Re[\beta_{ut}^\gamma(\beta_{ut}^Z)^*]$
	FH10 $Re[\beta_{ut}^g\bar{\eta}^*]$	GH10 $Re[\beta_{ut}^\gamma\eta^*]$
	FH11 $Im[\alpha_{ut}^Z\beta_{tu}^g]$	GH11 $Re[\beta_{ut}^\gamma\bar{\eta}^*]$
	FH12 $Re[\beta_{tu}^g(\beta_{tu}^Z)^*]$	GH12 $Im[\alpha_{ut}^Z\beta_{tu}^\gamma]$
	FH13 $Im[\theta\beta_{tu}^g]$	GH13 $Im[\beta_{tu}^\gamma(\alpha_{tu}^Z)^*]$
		GH14 $Re[\beta_{tu}^\gamma(\beta_{tu}^Z)^*]$
		GH15 $Im[\theta\beta_{tu}^\gamma]$

Table 3.4: Anomalous constants from the Gluon-Photon, Gluon-Z and Photon-Z channel results.

F1 is shown in equation (3.41)

$$\begin{aligned}
\langle T_1 T_1^\dagger \rangle &= F1 \times \alpha_{ut}^g (\alpha_{ut}^g)^* + F2 \times \alpha_{tu}^g (\alpha_{tu}^g)^* + \dots + G1 \times \alpha_{ut}^\gamma (\alpha_{ut}^\gamma)^* + \dots \\
&+ H1 \times \alpha_{ut}^Z (\alpha_{ut}^Z)^* + FG1 \times \text{Re}[\alpha_{ut}^g (\alpha_{ut}^\gamma)^*] + \dots \\
&+ FH1 \times \text{Re}[\alpha_{ut}^g (\alpha_{ut}^Z)^*] + \dots + GH15 \times \text{Im}[\theta \beta_{tu}^\gamma] \quad (3.40)
\end{aligned}$$

$$\begin{aligned}
F1 &= \frac{1}{27\Lambda^4} (2g_S^2 (2(4m_t - s)s + \\
&\quad - \frac{3(m_t^2 - t)(m_t^4 - 2m_t^2 s + 2s^2 + 2(m_t^2 + s)t + t^2)}{t} + \\
&\quad - \frac{3(s+t)(4m_t^4 + s^2 + t^2 - 4m_t^2(s+t))}{m_t^2 - s - t})). \quad (3.41)
\end{aligned}$$

The next step is the integration of these expressions to obtain the cross section for $t + q$ production at LHC.

3.2 Processes 6 to 8

For processes 6 to 8 we have, unlike for processes 1 to 5, SM diagrams that compete with the FCNC one's. With this possibility the contribution to the total cross section from these processes has terms in a different scale of energy. We can see this if we consider equation (2.1). For processes 1 to 5 there are no SM diagrams at tree level that can interfere with the FCNC ones. As a result the dependence on the energy scale in this case is $\frac{1}{\Lambda^4}$ (one $\frac{1}{\Lambda^2}$ factor from each diagram). This happens because we have only considered the $\frac{1}{\Lambda^2} \mathcal{L}^6$ term of the general Lagrangian. For processes 6 to 8 we have diagrams from the first term of the Lagrangian, \mathcal{L}_{SM} , that compete, and therefore interfere, with the $\frac{1}{\Lambda^2} \mathcal{L}^6$ term. This means that the lowest order contribution to the cross section is the one of order $\frac{1}{\Lambda^2}$. For processes 6 to 8 only the contribution from the $\frac{1}{\Lambda^2}$ term was considered. The terms in $\frac{1}{\Lambda^4}$ come from the dimension 6 Lagrangian but also from the interference between the dimension 8 Lagrangian term $\frac{1}{\Lambda^4} \mathcal{L}^8$ and the SM one. Since we are just considering the expansion to order 6 we just consider the interference terms. Apart this detail, the calculation follows the same line of the previous processes.

3.2.1 Process 6

The u coupling contribution for this process is described by $q\bar{q} \rightarrow t\bar{u}$, with q being a d, s or b quark, and is shown in figures (3.10) and (3.11). Like

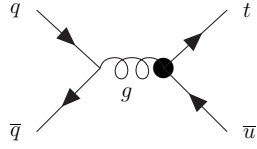


Figure 3.10: FCNC Feynman diagram of process 6 for the strong sector.

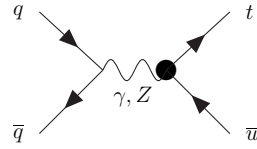


Figure 3.11: FCNC Feynman diagram of process 6 for the electroweak sector.

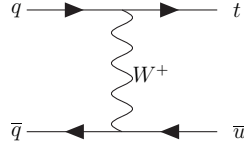


Figure 3.12: SM Feynman diagram for process 6.

explained before we must consider the SM diagram of figure (3.12). The transition amplitudes for FCNC are represented in equations (3.42)-(3.44).

$$iT_g^s = [\bar{u}_t^i V_g^\mu(-p_3, p_4, p_3 + p_4) 2t_{ij}^a v_3^j] \left(\frac{-ig_{\mu\nu}}{s} \right) [\bar{v}_2^k i g_3 t_{kl}^a \gamma^\nu u_1^l] \quad (3.42)$$

$$iT_\gamma^s = [\bar{u}_t^i V_\gamma^\mu(-p_3, p_4, p_3 + p_4) \delta_{ij} v_3^j] \left(\frac{-ig_{\mu\nu}}{s} \right) [\bar{v}_2^k i e Q_d \gamma^\nu \delta_{kl} u_1^l] \quad (3.43)$$

$$iT_Z^s = [\bar{u}_t^i V_z^\mu(-p_3, p_4, p_3 + p_4) \delta_{ij} v_3^j] \left(\frac{-i}{s - m_z^2} \right) \left(g_{\mu\nu} - \frac{k_\mu k_\nu}{m_z^2} \right) [\bar{v}_2^k \frac{ie}{\sin(2\theta_w)} \gamma_\nu [T_3 - 2Q_d^2 \sin^2(\theta_w) - T_3 \gamma_5] \delta_{kl} u_1^l]. \quad (3.44)$$

One must notice that for this case, like for process 7 and 8, the constant T_3 has a value equal to $-\frac{1}{2}$. For the SM diagram we have:

$$iT_W^t = [\bar{u}_t^i i g \frac{\sqrt{2}}{2} \gamma^\mu \gamma_L V_{dt} \delta_{ij} u_1^j] \left(\frac{-i}{t - m_w^2} \right) \left(g_{\mu\nu} - \frac{k_\mu k_\nu}{m_w^2} \right) [\bar{v}_2^k i g \frac{\sqrt{2}}{2} \gamma^\nu \gamma_L V_{du} \delta_{kl} v_3^l]. \quad (3.45)$$

Now we just want the interference between the FCNC and SM diagrams.

Gluon and W interference

$$\begin{aligned}
\langle T_w^t (T_g^s)^\dagger \rangle &= \frac{1}{4 \times 9} \frac{i2g_3 g^2 V_{dt} V_{du}}{2s(t - m_w^2)} Tr[t^a t^a] \\
&\quad \times Tr[(\not{p}_4 + m_t) \cdot \gamma^\mu \cdot \gamma_L \cdot \not{p}_1 \cdot \gamma_\alpha \cdot \not{p}_2 \cdot F_\mu(p_4 - p_1) \cdot \not{p}_3 \cdot \\
&\quad \cdot \bar{V}_g^\alpha(-p_3, p_4, p_3 + p_4)] \quad (3.46)
\end{aligned}$$

$$\begin{aligned}
\langle T_g^s (T_w^t)^\dagger \rangle &= \frac{1}{4 \times 9} \frac{-i2g_3 g^2 V_{dt}^* V_{du}^*}{2s(t - m_w^2)} Tr[t^a t^a] \\
&\quad \times Tr[(\not{p}_4 + m_t) \cdot V_g^\alpha(-p_3, p_4, p_3 + p_4) \cdot \not{p}_3 \cdot \bar{F}_\mu(p_4 - p_1) \cdot \\
&\quad \cdot \not{p}_2 \cdot \gamma_\alpha \cdot \not{p}_1 \cdot \gamma_R \cdot \gamma^\mu]. \quad (3.47)
\end{aligned}$$

Photon and W interference

$$\begin{aligned}
\langle T_w^t (T_\gamma^s)^\dagger \rangle &= \frac{1}{4 \times 9} \frac{ieg^2 V_{dt} V_{du} Q_d}{2s(t - m_w^2)} Tr[\delta] \\
&\quad \times Tr[(\not{p}_4 + m_t) \cdot \gamma^\mu \cdot \gamma_L \cdot \not{p}_1 \cdot \gamma_\alpha \cdot \not{p}_2 \cdot \bar{F}_\mu(p_4 - p_1) \cdot \not{p}_3 \cdot \\
&\quad \cdot \bar{V}_\gamma^\alpha(-p_3, p_4, p_3 + p_4)] \quad (3.48)
\end{aligned}$$

$$\begin{aligned}
\langle T_\gamma^s (T_w^t)^\dagger \rangle &= \frac{1}{4 \times 9} \frac{-ieg^2 V_{dt}^* V_{du}^* Q_d}{2s(t - m_w^2)} Tr[\delta] \\
&\quad \times Tr[(\not{p}_4 + m_t) \cdot V_\gamma^\alpha(-p_3, p_4, p_3 + p_4) \cdot \not{p}_3 \cdot F_\mu(p_4 - p_1) \cdot \\
&\quad \cdot \not{p}_2 \cdot \gamma_\alpha \cdot \not{p}_1 \cdot \gamma_R \cdot \gamma^\mu]. \quad (3.49)
\end{aligned}$$

Z and W interference

$$\begin{aligned}
\langle T_w^t (T_z^s)^\dagger \rangle &= \frac{1}{4 \times 9} \frac{ieg^2 V_{dt} V_{du}}{4(s - m_z^2)(t - m_w^2) s_w c_w} Tr[\delta] \\
&\quad \times Tr[(\not{p}_4 + m_t) \cdot \gamma^\mu \cdot \gamma_L \cdot \not{p}_1 \cdot \bar{\Gamma}_\alpha(p_3 + p_4) \cdot \not{p}_2 \cdot F_\mu(p_4 - p_1) \cdot \not{p}_3 \cdot \\
&\quad \cdot \bar{V}_z^\alpha(-p_3, p_4, p_3 + p_4)] \quad (3.50)
\end{aligned}$$

$$\begin{aligned}
\langle T_z^s (T_w^t)^\dagger \rangle &= \frac{1}{4 \times 9} \frac{-ieg^2 V_{dt}^* V_{du}^*}{4(s - m_z^2)(t - m_w^2) s_w c_w} Tr[\delta] \\
&\quad \times Tr[(\not{p}_4 + m_t) \cdot V_z^\alpha(-p_3, p_4, p_3 + p_4) \cdot \not{p}_3 \cdot \bar{F}_\mu(p_4 - p_1) \cdot \\
&\quad \cdot \not{p}_2 \cdot \Gamma_\alpha(p_3 + p_4, Q_d) \cdot \not{p}_1 \cdot \gamma_R \cdot \gamma^\mu]. \quad (3.51)
\end{aligned}$$

3.2.2 Results

For this process, as for the 7th and the 8th, we have simpler results in comparison to the first 5 processes. For all processes we have 5 terms, each one dependent on two Mandelstam variables, t and s . Another difference comes from the fact that we are calculating the interferences with the SM channels shown above. This introduces the CKM constants. In table (3.5) we can see the anomalous couplings associated with the five terms. Since here we are dealing with one anomalous vertex we just have one anomalous constant. We introduce a new label, I , associated to the W channel. Like

Gluon-W	Photon-W	Z-W
$FI1 \text{ Re}[\beta_{ut}^S]$	$GI1 \text{ Re}[\beta_{ut}^\gamma]$	$HI1 \text{ Re}[\beta_{ut}^Z]$
		$HI2 \text{ Re}[\eta]$
		$HI3 \text{ Re}[\bar{\eta}]$

Table 3.5: Anomalous constants from the Gluon-W, Photon-W and Z-W channel results.

before we show in equation (3.52) the result for the process 6. In equation (3.53) we have the term $FI1$ for this process.

$$\begin{aligned} \langle T_6 T_6^\dagger \rangle &= FI1 \times \text{Re}[\beta_{ut}^S] + GI1 \text{Re}[\beta_{ut}^\gamma] + \\ &\quad + HI1 \text{Re}[\beta_{ut}^Z] + HI2 \times \text{Re}[\eta] + HI3 \times \text{Re}[\bar{\eta}] \end{aligned} \quad (3.52)$$

$$FI1 = \frac{16g_w^2 g_3 m_t (s + t - m_t^2) v V_{td} V_{ud}}{9(m_w^2 - t)\Lambda^2}. \quad (3.53)$$

Chapter 4

From partons to protons

4.1 PDF

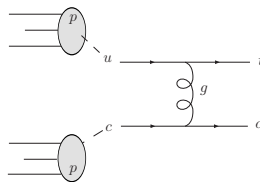


Figure 4.1: Pictorial view of a collision at the LHC.

As mentioned earlier, we want to calculate the cross section of $pp \rightarrow tq$ from the parton level cross section $qq \rightarrow tq$. In figure (4.1) we can see a pictorial view of these processes. We start with two protons, each one with tetra-momentum P_1 and P_2 , colliding with a centre of mass energy S (expected to be $\sqrt{14}$ Tev at LHC). From the protons we must extract two partons producing, for the case under study, one top quark and a light quark. For the cross section calculation we define new variables x_i , ($0 \leq x_i \leq 1$), as the fraction of the parton's q_i momentum, p_i , with respect to the proton momentum, P_i :

$$\begin{aligned}\vec{p}_{q_1} &= x_1 \vec{P}_1 \\ E_{q_1} &= x_1 E_1 \\ \vec{p}_{q_2} &= x_2 \vec{P}_2 \\ E_{q_2} &= x_2 E_2.\end{aligned}\tag{4.1}$$

We need to establish the relation between the proton-proton centre of mass energy and the parton-parton collision. From equation (4.1) to equation (4.3), and considering the two incoming particles with negligible mass, we have equation (4.4)

$$S = (P_1 + P_2)^2 = m_{P_1}^2 + m_{P_2}^2 + 2P_1 \cdot P_2 \sim 2P_1 \cdot P_2 \quad (4.2)$$

$$s = (p_1 + p_2)^2 = m_{q_1}^2 + m_{q_2}^2 + 2p_1 \cdot p_2 \sim 2p_1 \cdot p_2 \quad (4.3)$$

$$s = x_1 x_2 S. \quad (4.4)$$

The total cross section for $pp \rightarrow tq$ is the integration of the parton differential cross section over the values of x_1 and x_2 , convoluted with the probability to extract partons q_1 and q_2 , with momentum p_1 and p_2 ,

$$\begin{aligned} \sigma_{pp \rightarrow tq_3} &= \int_0^1 \int_0^1 dx_1 dx_2 f_1(x_1, q_1, Q^2) f_2(x_2, q_2, Q^2) \\ &\quad \times \int_{t_{max}}^{t_{min}} dt \frac{d\sigma(s,t)}{dt} \Big|_{q_1 q_2 \rightarrow tq_3}. \end{aligned} \quad (4.5)$$

In equation (4.5) the functions $f_i = f(x_i, q_i, Q^2)$, $i = 1, 2$ are the Parton Density Functions (PDF). They give the probability to extract a parton q_i , with momentum $p_i = x_i P_i$ from a proton, in a collision with a momentum transfer Q^2 . The PDF version we use is the one from the CTEQ group (see [9] for details). For the actual calculation we use a Mathematica version of CTEQ5M [10]. Since the minimum energy required for these processes is the top quark mass, the scale of the Q^2 was set to $175 \text{ GeV}/c^2$. In figure (4.2) the PDF used for the u, d, and c quarks and for the gluon are shown as a function of x_i . Notice that for values of x_i below 10^{-1} the gluon has a greater probability density.

4.2 Kinematical limits

The limits for the Mandelstam variables are determined from the kinematical constraints. Following the momentum definition of figure (3.5) and choosing the centre of mass frame we have:

$$E_{total} = \sqrt{s} = E_1 + E_2 \sim |\vec{p}_1| + |\vec{p}_2| \quad (4.6)$$

and since $E_1 = E_2$,

$$\begin{cases} E_1 = \frac{\sqrt{s}}{2} \text{ and } |\vec{p}_1| = \frac{\sqrt{s}}{2} \\ E_2 = \frac{\sqrt{s}}{2} \text{ and } |\vec{p}_2| = \frac{\sqrt{s}}{2} \end{cases}$$

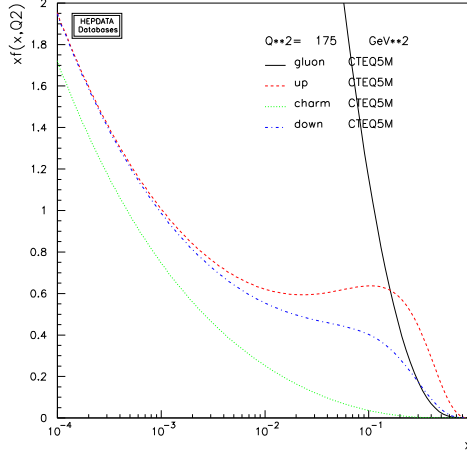


Figure 4.2: Quarks up, down, charm and gluon PDF functions for CTEQ5M. Plots from [11].

Therefore we can write the particle's tetra-momentum as:

$$\left\{ \begin{array}{l} p_1 = \left(\frac{\sqrt{s}}{2}, 0, 0, \frac{\sqrt{s}}{2} \right) \\ p_2 = \left(\frac{\sqrt{s}}{2}, 0, 0, -\frac{\sqrt{s}}{2} \right) \\ p_3 = (E_3, -\vec{p}_T, -|\vec{p}_t| \cos \theta) \\ p_4 = (E_t, \vec{p}_T, |\vec{p}_t| \cos \theta) \end{array} \right.$$

where \vec{p}_t is the top quark momentum and \vec{p}_T the top quark transverse momentum. From momentum and energy conservation we obtain:

$$\left\{ \begin{array}{l} t = m_t^2 - 2 \left(\frac{\sqrt{s}}{2} \frac{s+m_t^2}{2\sqrt{s}} - \frac{\sqrt{s}}{2} \frac{s-m_t^2}{2\sqrt{s}} \cos \theta \right) \\ s = m_t^2 + 2|\vec{p}_T|^2 + \sqrt{(m_t^2 + 2|\vec{p}_T|^2)^2 - m_t^4} \end{array} \right.$$

with,

$$\left\{ \begin{array}{l} \cos \theta = \pm \sqrt{1 - \frac{|\vec{p}_T|^2}{|\vec{p}_t|^2}} \\ |\vec{p}_t| = \frac{s-m_t^2}{2\sqrt{s}} \end{array} \right.$$

Finally, the limits for t and s are imposed through the definition of a cut off on the transverse momentum of the final state partons. For the present work we set the minimum transverse momentum of the top quark to $|\vec{p}_{T_{min}}| = 15 \text{ GeV}/c^2$.

Chapter 5

Results and discussion

To obtain the cross sections we used a random number generator to produce a set of possible anomalous coupling constants values. We have generated two random values for each constant, x and y , where $0 \leq x \leq 8$ and $0 \leq y \leq 2\pi$. Each constant has the structure $10^{-x}e^{iy}$, where the real and the imaginary part runs from -1 to 1. The top quark branching ratios [8] and the cross section depend on the same anomalous constants which allows the direct comparison of the FCNC branching ratios with the cross sections. Instead of determining the variation of the cross sections with respect to the anomalous couplings, we have the possibility to infer about the dependence of the branching ratios with the production cross sections. This allows, for example, to correlate limits on the FCNC branching ratios with limits on the single-top production FCNC cross section. This is a major point in our full analysis since the branching ratios will be measured or limited in the first year of luminosity with the $t\bar{t}$ experimental data. This means that we may extract information about the possible experimental limits for the production cross section of FCNC single-top with $t\bar{t}$ experimental data.

All values of the physical constants were taken from the Particle Data Group [12].

5.1 Processes 1 to 5

The results presented in this chapter are the sum of all cross sections from the five processes including the contribution from both u and c couplings. This gives the single-top production cross section through $qq \rightarrow tq$, with q being a u or a c quark. The sum of the u and c cross sections was done since experimentally it is not possible to distinguish a u quark from c quark.

This is not the case for a b quark, where there is an experimental technique (b-tag) that allows to identify a jet from the hadronization of a b quark in the final state. This is the reason why we have separated in the processes 7 and 8, the ones involving a b quark in the final products, i.e., $qb \rightarrow tb$ and $q\bar{b} \rightarrow t\bar{b}$.

Like explained above, we want to determine the possible values for the cross sections with respect to the FCNC top quark decay branching ratios, i.e., plots of the form: cross section versus $BR(t \rightarrow qx)$, where x is a gluon, a photon or a Z. We will also show cross sections versus $BR(t \rightarrow qX)$, where in this case we are working with the sum of all branching ratios. All plots were generated according to the condition $BR(t \rightarrow tg) < 10^{-2}$, $BR(t \rightarrow t\gamma) < 10^{-2}$ and $BR(t \rightarrow tZ) < 10^{-2}$. These constraints are stronger but close to the known experimental constraints to date.

In figure (5.1) the results for the cross section with respect to the FCNC top quark decay branching ratio, $BR(t \rightarrow qg)$, are shown. The plot is in logarithmic scale and the cross section is in picobarns. In figures (5.2) and (5.3) the equivalent results are shown as a function of the FCNC top quark decay branching ratios $BR(t \rightarrow q\gamma)$ and $BR(t \rightarrow qZ)$, respectively. We see that for all plots the contribution for the total cross sections is not negligible compared with the SM single-top production of ~ 300 pb [13, 14, 15]. This contribution is, for figure (5.2) and (5.3), limited by a constant upper bound in the cross section of around 100 pb. Note however that 100 pb should be seen as an order of magnitude. Had we generated more points we would pick up larger values for the cross section. This is not the case for the first plot. Here the upper bound is not the same for all values of the $t \rightarrow qg$ branching ratio. For values bellow 10^{-4} we note that the cross section is limited to around 10 pb. Hence, contributions to the total cross section higher than 10 pb imply that the $t \rightarrow qg$ branching ratio must be above 10^{-4} . This is an interesting point because it will be tested at the LHC. In the first year of operation, in the absence of signal, a 95% confidence level limit for $BR(t \rightarrow qg)$ is expected to be set at of 10^{-3} [16], just close to the example given.

In figure (5.4) we show the cross section as a function of the sum of all three branching ratios considered before. It was constructed using the values of the cross section with respect to the sum of all three branching ratios considered before. This means that in this plot we work with the branching ratio $BR(t \rightarrow qX)$, where q is a u or a c quark and X is a gluon, a photon or a Z. Like before the scale is logarithmic and the cross section is in picobarn. Here we can see a different picture from the three previous plots. Instead of a horizontal upper bound we have sloped bands. This

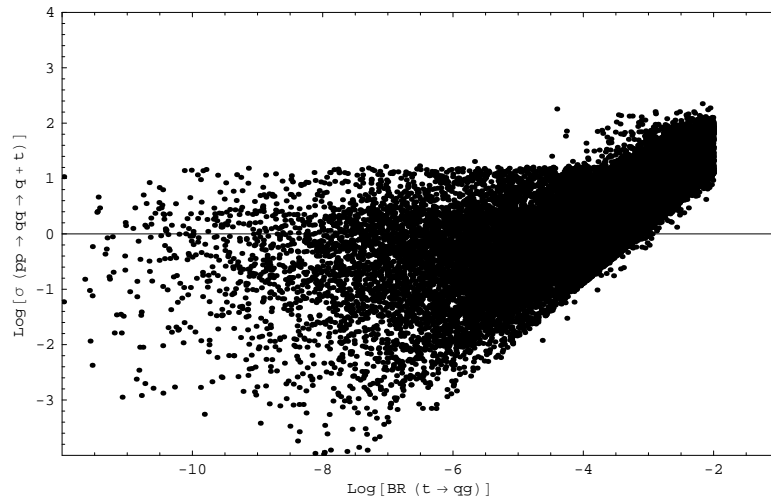


Figure 5.1: Cross section for the processes $qq \rightarrow tq$ as a function of the branching ratio $BR(t \rightarrow qq)$.

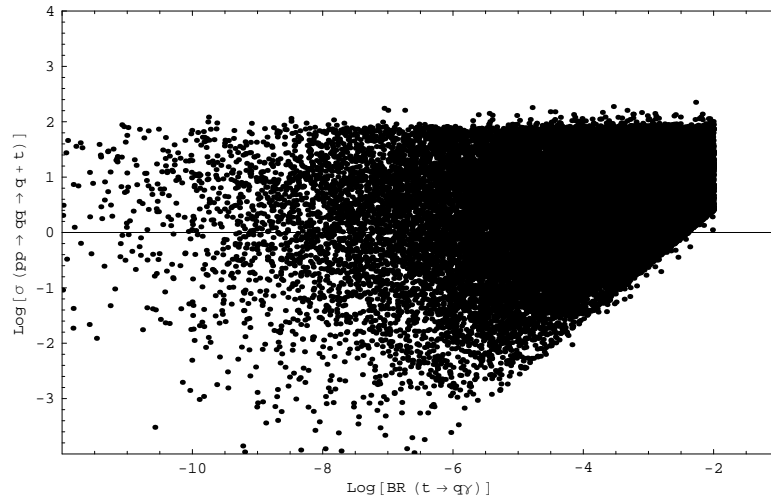


Figure 5.2: Cross section for the processes $qq \rightarrow tq$ as a function of the branching ratio $BR(t \rightarrow q\gamma)$.

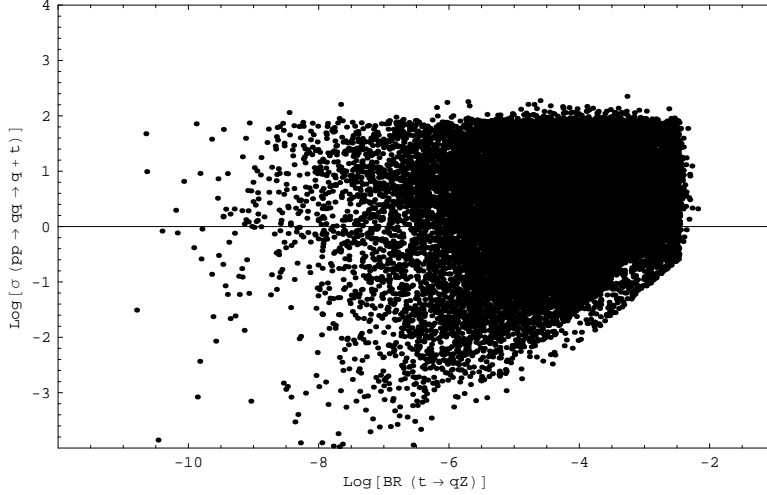


Figure 5.3: Cross section for the processes $qq \rightarrow tq$ as a function of the branching ratio $BR(t \rightarrow qZ)$.

means that we have an additional constraint in the contribution for the total cross section. Nevertheless it still allows for contributions of around 10 pb for total branching ratios below 10^{-4} . This plot is interesting since it suggests a different experimental analysis. With this plot we can study possible experimental limits for the cross section as a function of the $t \rightarrow qX$ branching ratio without making any distinction between the electroweak and strong top quark branching ratios.

Since we have a set of values distributed by sloped regions it is possible, by using the branching ratio limits, to infer a limit on the cross section. For example, if we had a limit of $\sim 10^{-4}$ for the branching ratio, we would expect a limit of around 10 pb for this production channel, as can be seen in figure (5.5). Besides that, if we additionally set experimental limits for the cross section, we can constrain the possible domain for the anomalous constants. For example, from figure (5.5) we can see that if we had in addition to the 10^{-4} branching ratio limit, a limit in the cross section of ~ 50 pb, we would be excluding some regions for the FCNC couplings. We note that one dedicated analysis for the expected limit in the branching ratio of FCNC top quark decay to light jet and one X particle, with this X being a gluon, a photon or a Z, was not yet done.

Finally, we remind that these results are only for one of the possible channels of t+jet production ($qq \rightarrow tq$ in table (1.2)). Since experimen-

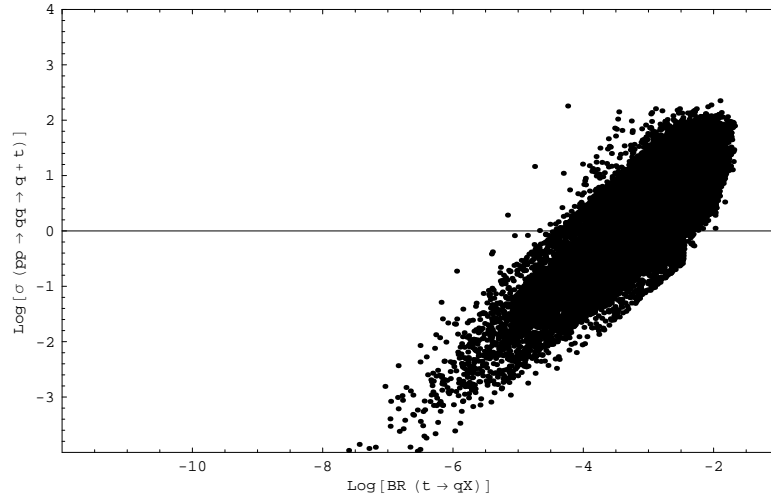


Figure 5.4: Cross section for the processes $qq \rightarrow tq$ as a function of the branching ratio $BR(t \rightarrow qX)$. The X particle can be a gluon, a photon or a Z.

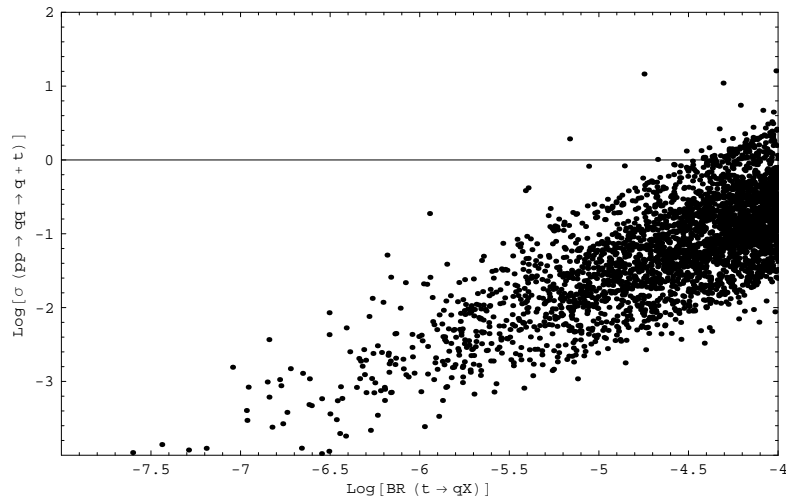


Figure 5.5: Cross section for the processes $qq \rightarrow tq$ as a function of the branching ratio $BR(t \rightarrow qX)$ rescaled.

tally what is observed is the top + jet channel, we need to generate the equivalent plots for the remaining production channels and from the sum of all the contributions try to infer if the above analysis holds with the new contributions. The remaining processes considered were $gq \rightarrow tg$, $gg \rightarrow tq$ and $qq \rightarrow t$, which will be referred to as gluon processes. The cross section for these processes was calculated in [2]. In figure (5.6) the gluon processes contribution for the total cross section with respect to the FCNC top quark gluon branching ratio is shown. The plot is in logarithmic scale, the cross section is in picobarns and the previous sample of anomalous coupling constants was used. As expected, there is an evident linearity dependence of the cross section with the branching ratio [2]. In comparison with the previous results we note that these gluon processes give a larger contribution to the cross section for higher values of the $t \rightarrow qg$ branching ratio. As we can see, for values of $BR(t \rightarrow qg) > 10^{-4}$ the gluon processes can reach cross sections of the order of 10^3 , while for the $qq \rightarrow tq$ channel, the cross section is $\sim 10^2$. On the contrary for $BR(t \rightarrow qg) < 10^{-4}$ the cross section contribution for the $qq \rightarrow tq$ channel can reach a constant value of 10 pb (as noted above), while for the gluon channel the possible contribution decrease with the branching ratio. Therefore, one first conclusion is that if we measure a single-top production via FCNC of about 10 pb, and also a FCNC branching ratio $BR(t \rightarrow qg)$ of less than 10^{-4} , the cross section is mainly dominated by the $qq \rightarrow tq$ production channel. Finally in figure (5.7) we shown the equivalent plot with the sum of all cross section production channels. As expected it is a sum of the plots of figure (5.1) and (5.6).

In figure (5.8) and (5.9) we can see the behaviour of the total cross section with respect to the $t \rightarrow q\gamma$ and $t \rightarrow qZ$ branching ratios, respectively. We note that the comparison with figures (5.2) and (5.3) shows we have now larger values for the total cross section. We still have a horizontal bound that for this case is of the order of $\sim 10^3$ pb. Analysing figure (5.7) we can understand the origin of this extra contribution for the cross section with respect to the 10^2 pb bound of figure (5.2) and (5.3). Since now we are working with the gluon processes, this contribution comes from the region where $BR(t \rightarrow qg) > 10^{-4}$ in figure (5.7). Therefore we have to pay special attention to this region since its points have a very high $t \rightarrow qg$ branching ratio.

In figure (5.10) the total cross section with respect to the $t \rightarrow qX$ decay branching ratios is shown. As before, the sum of all three branching ratios is represented. As for figure (5.4), the introduction of the electroweak channel brings one additional constraint to the cross section. We also note that the bound on the $t \rightarrow qX$ branching ratio still sets a limit of ~ 10 pb on the

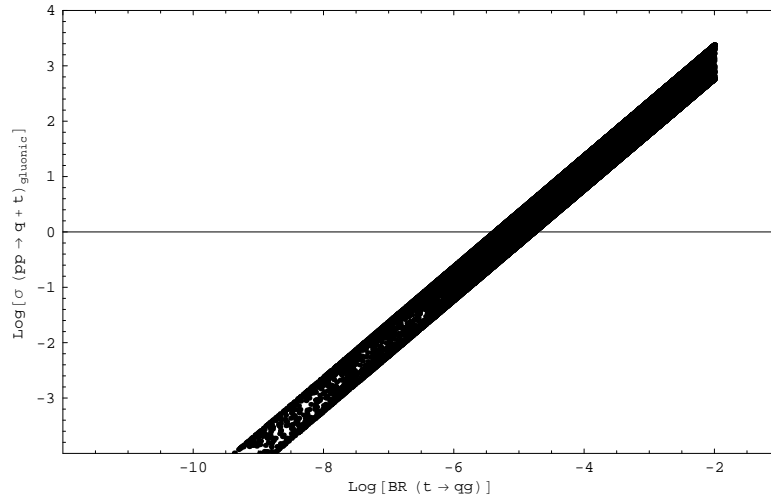


Figure 5.6: Gluon processes cross section as a function of the $BR(t \rightarrow qq)$.

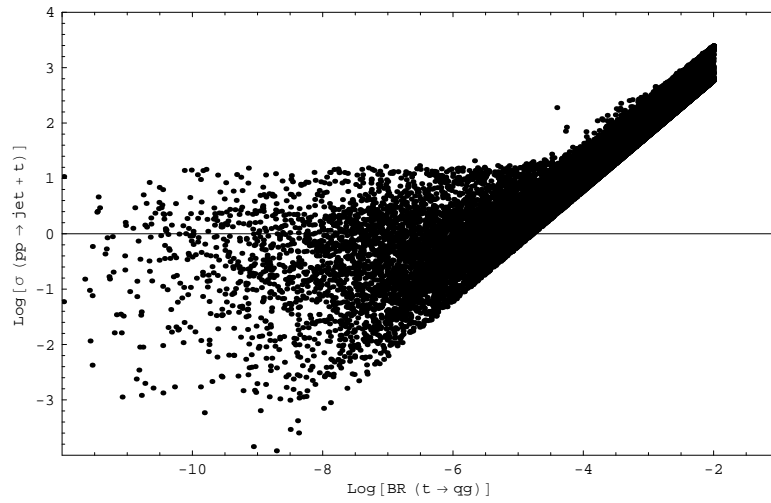


Figure 5.7: Total cross section for the processes $pp \rightarrow t + jet$ as function of the branching ratio $BR(t \rightarrow qq)$.

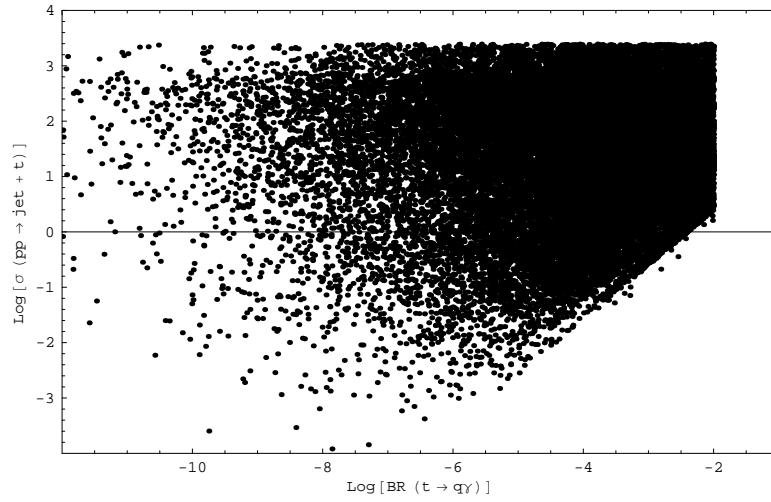


Figure 5.8: Total cross section for the processes $pp \rightarrow t + jet$ as function of the branching ratio $BR(t \rightarrow q\gamma)$.

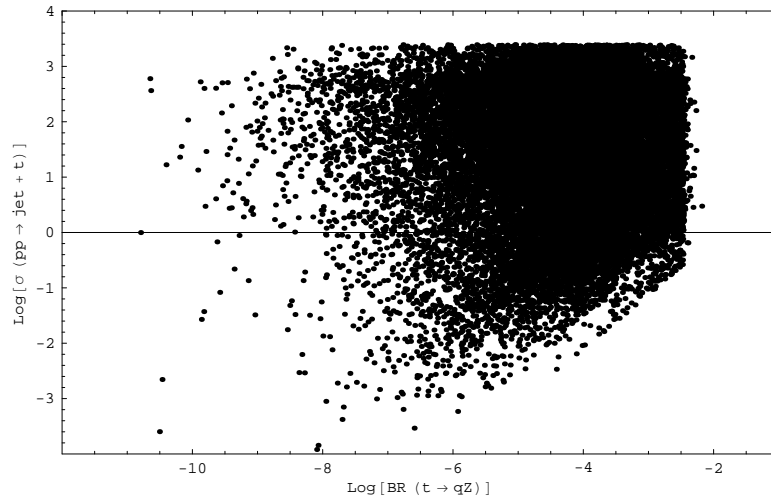


Figure 5.9: Total cross section for the processes $pp \rightarrow t + jet$ as function of the branching ratio $BR(t \rightarrow qZ)$.

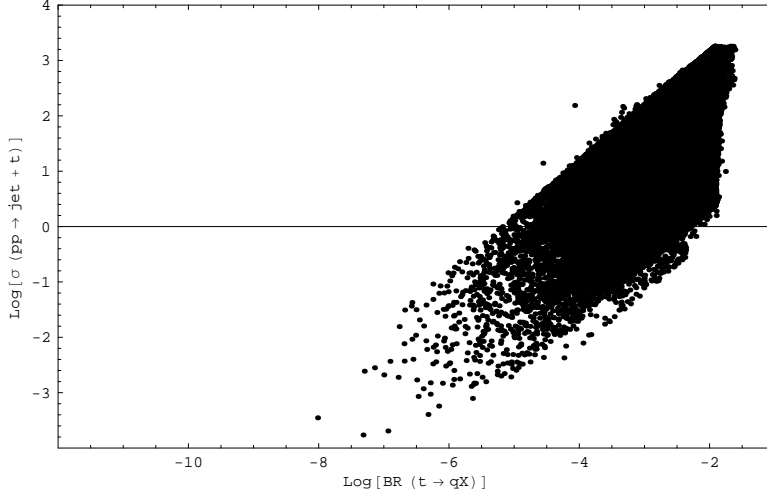


Figure 5.10: Total cross section for the processes $pp \rightarrow t + jet$ as function of the branching ratio $BR(t \rightarrow qX)$. The X particle is a gluon, a photon or a Z.

cross section.

Finally in figure (5.11) the strong contribution for the $qq \rightarrow tq$ production channel with respect to the FCNC gluon top decay branching ratio is shown. From the "single-top production" chapter we can see that this corresponds to the contribution of the first seven terms for the cross section. Therefore in this plot we try to quantify the contribution of the strong sector with respect to the electroweak sector (including interferences) for the total cross section. The comparison with figure (5.1) shows that the strong contribution for the cross section dominates the region where the $t \rightarrow qq$ branching ratios are above $\sim 10^{-4}$. For lower values we see that the contribution is dominated by the electroweak and interference channels. As an example we extracted one particular point from this zone in figure (5.1) and calculated the contribution from each sector. The results are shown in table (5.1). The main contribution comes from the photon sector and the second largest contribution from the interference between the photon and Z sectors. The strong sector contribution is, for this case, negligible. The main cause is the lower values of the strong anomalous constants in comparison with the electroweak ones. As a consequence the branching ratios are also very different (table (5.2)). In figure (5.12) the electroweak channel contribution for the cross section with respect to the sum of the electroweak FCNC top

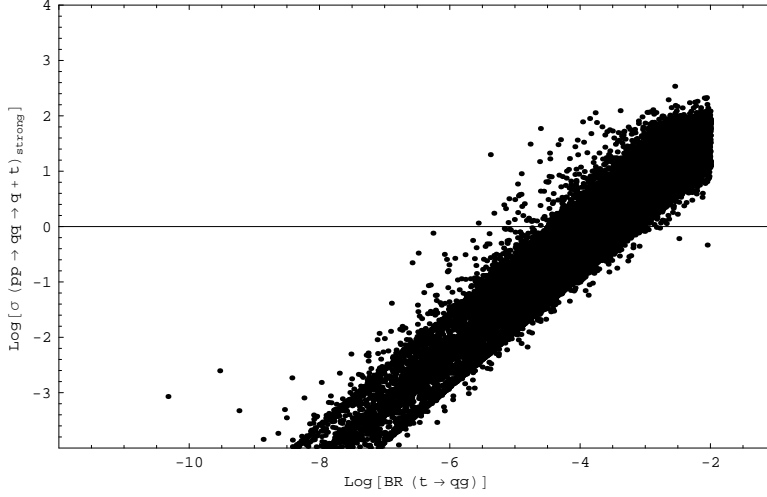


Figure 5.11: Strong sector cross section for processes $qq \rightarrow tq$ as a function of the branching ratio $BR(t \rightarrow qq)$.

decay branching ratios ($BR(t \rightarrow q\gamma) + BR(t \rightarrow qZ)$) is shown. This plot confirms the previous results. The large values for the cross section come from the large values of the electroweak branching ratios.

Sector	Cross section (pb)
Gluon	4.639×10^{-7}
Photon	12.104
Z	0.353
Gluon-Photon	2.221×10^{-4}
Gluon-Z	-1.619×10^{-5}
Photon-Z	1.677
Total	14.134

Table 5.1: Cross section contributions of the different sectors for one specific point.

Decay	Branching ratio
$t \rightarrow tg$	9.613×10^{-11}
$t \rightarrow t\gamma$	9.171×10^{-3}
$t \rightarrow tZ$	5.062×10^{-4}

Table 5.2: Branching ratios for one specific point.

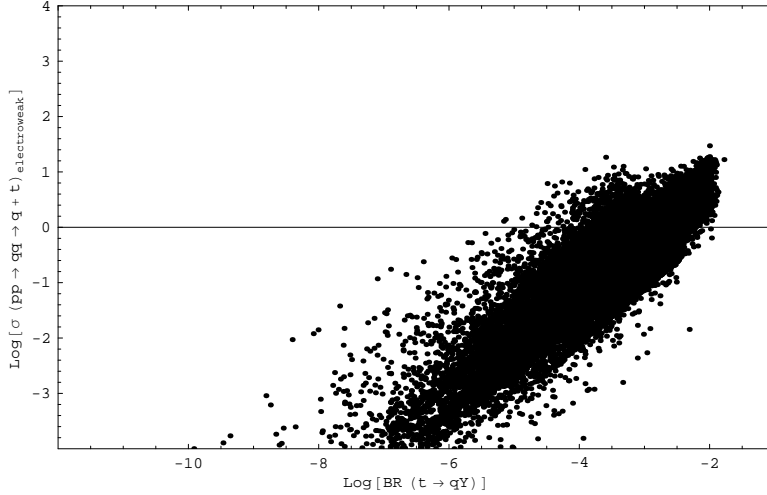


Figure 5.12: Electroweak and interferences sector cross section for processes $qq \rightarrow tq$ as a function of the branching ratio $BR(t \rightarrow qY)$. The Y particle can be a photon or a Z.

5.2 Processes 6 to 8

For these processes the method follows the same principle as the previous ones. As explained before we separated the processes with a b quark in the final state from the other ones. The values for the cross section are negligible when compared to the strong sector ones. In figure (5.13) the cross section for the sum of the processes 6 to 8, excluding the two b-processes referred, with respect to the $t \rightarrow qg$ branching ratio is shown. The sum of the remaining b-processes cross section with respect to the $t \rightarrow qg$ branching ratio is shown in figure (5.14). The plots are, like before, in logarithmic scale and the cross section is in picobarns. We note that these contributions are extremely small. The cross section has a maximum at around 0.1 pb.

We should keep in mind that we are dealing with the interference with the SM diagrams. The main reason for these results is a highly suppressed mixing from the off-diagonal CKM matrix elements as well as small PDF contributions for the incoming quarks. Since this was already observed in [2] we have decided not to show any more plots for these processes.

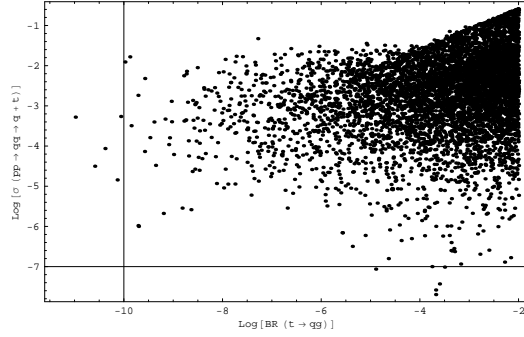


Figure 5.13: Cross section for processes $qq \rightarrow tq$ as a function of the branching ratio $BR(t \rightarrow qq)$. Processes with b quarks as final products were not considered.

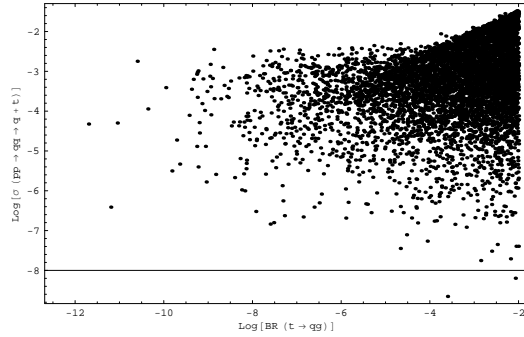


Figure 5.14: Cross section for processes $qb \rightarrow tb + q\bar{b} \rightarrow t\bar{b}$ as a function of the branching ratio $BR(t \rightarrow qq)$.

Chapter 6

Conclusions

The calculation of FCNC single-top production through the $qq \rightarrow tq$ channel is complete. We conclude that for higher values of the $t \rightarrow qg$ branching ratio the contribution from this production channel is comparable to the production from gluon processes and that the new electroweak contributions can reach high cross section values for lower $t \rightarrow qg$ branching ratio values. With the introduction of the electroweak sector we have completed the study of FCNC for top + jet production which allowed new physical analysis.

With the $qq \rightarrow tq$ production channel completed we constructed a new study case: the dependence of the cross section with the FCNC top decay branching ratio, $t \rightarrow qX$, where X can be a gluon, a photon or a Z. A dedicated analysis for this type of branching ratio could correlate experimental limits for total t+jet single-top FCNC cross section with the FCNC branching ratios experimental limits. This is a relevant point since with this method it could be possible to infer about experimental limits for the FCNC single-top cross section through $t\bar{t}$ experimental data.

We also concluded that possible contributions from the processes 6 to 8 are negligible. Therefore if FCNC contributions for the single-top production are measured at the LHC, they probably will come from the Λ^{-4} term of the full Lagrangian.

Finally, with the calculation of all analytical expressions, we are now able to introduce these FCNC single-top production contributions into a Monte Carlo generator, which allows additional experimental studies of FCNC interactions.

The results presented here will soon be submitted to publication in a scientific journal.

Appendix A

Processes 2 to 8

A.1 Process 2

Process 2 is $uc \rightarrow tc$ (u coupling) (figures A.1 and A.2). For this process we just have the contribution from one t channel. The transition amplitudes for gluon, photon and Z are

$$iT_g^t = [\bar{u}_t^i V_g^\mu(p_1, p_4, p_4 - p_1) 2t_{ij}^a u_1^j] \left(\frac{-i g_{\mu\nu}}{t} \right) [\bar{u}_3^k i g_3 t_{kl}^a \gamma^\nu u_2^l] \quad (\text{A.1})$$

$$iT_\gamma^t = [\bar{u}_t^i V_\gamma^\mu(p_1, p_4, p_4 - p_1) \delta_{ij} u_1^j] \left(\frac{-i g_{\mu\nu}}{t} \right) [\bar{u}_3^k i e Q_c \gamma^\nu \delta_{kl} u_2^l] \quad (\text{A.2})$$

$$iT_Z^t = [\bar{u}_t^i V_Z^\mu(p_1, p_4, p_4 - p_1) \delta_{ij} u_1^j] \left(\frac{-i}{t - m_Z^2} \right) \left(g_{\mu\nu} - \frac{k_\mu k_\nu}{m_Z^2} \right) [\bar{u}_3^k \frac{i e}{\sin(2\theta_w)} \gamma_\nu [T_3 - 2Q_c^2 \sin^2(\theta_w) - T_3 \gamma_5] \delta_{kl} u_2^l]. \quad (\text{A.3})$$

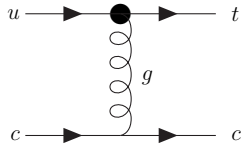


Figure A.1: Feynman diagram of process 2 for the strong sector.

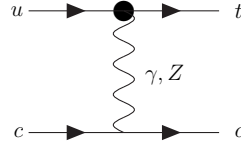


Figure A.2: Feynman diagram of process 2 for the electroweak sector.

The total transition amplitude is

$$iT_{total} = iT_g^t + iT_\gamma^t + iT_Z^t. \quad (\text{A.4})$$

Like before we separate the calculations into each boson channel and the respective interferences.

gluon

For the gluon channel we have

$$\begin{aligned} \langle T_g^t(T_g^t)^\dagger \rangle &= \frac{1}{4 \times 9} \frac{4g_3^2}{t^2} Tr[t^{ab}]Tr[t^{ab}] \\ &\times Tr[V_g^\alpha(p_1, p_4, p_4 - p_1) \cdot \not{p}_1 \cdot \bar{V}_g^\beta(p_1, p_4, p_4 - p_1) \cdot (\not{p}_4 + m_t)] \\ &\times Tr[\gamma_\alpha \cdot \not{p}_2 \cdot \gamma_\beta \cdot \not{p}_3]. \end{aligned} \quad (\text{A.5})$$

Photon

$$\begin{aligned} \langle T_\gamma^t(T_\gamma^t)^\dagger \rangle &= \frac{1}{4 \times 9} \left(\frac{eQ_c}{t}\right)^2 Tr[\delta]Tr[\delta] \\ &\times Tr[V_\gamma^\alpha(p_1, p_4, p_4 - p_1) \cdot \not{p}_1 \cdot \bar{V}_\gamma^\beta(p_1, p_4, p_4 - p_1) \cdot (\not{p}_4 + m_t)] \\ &\times Tr[\gamma_\alpha \cdot \not{p}_2 \cdot \gamma_\beta \cdot \not{p}_3]. \end{aligned} \quad (\text{A.6})$$

Z

$$\begin{aligned} \langle T_z^t(T_z^t)^\dagger \rangle &= \frac{1}{4 \times 9} \frac{e^2}{4s_w^2 c_w^2 (t - m_z^2)^2} Tr[\delta]Tr[\delta] \\ &\times Tr[V_Z^\alpha(p_1, p_4, p_4 - p_1) \cdot \not{p}_1 \cdot \bar{V}_Z^\beta(p_1, p_4, p_4 - p_1) \cdot (\not{p}_4 + m_t)] \\ &\times Tr[\Gamma_\alpha(p_4 - p_1, Q_c) \cdot \not{p}_2 \cdot \bar{\Gamma}_\beta(p_4 - p_1, Q_c) \cdot \not{p}_3]. \end{aligned} \quad (\text{A.7})$$

Gluon and Photon interference

$$\langle T_g^t(T_\gamma^t)^\dagger \rangle = \langle T_\gamma^t(T_g^t)^\dagger \rangle = 0. \quad (\text{A.8})$$

Gluon and Z interference

$$\langle T_g^t(T_z^t)^\dagger \rangle = \langle T_z^t(T_g^t)^\dagger \rangle = 0. \quad (\text{A.9})$$

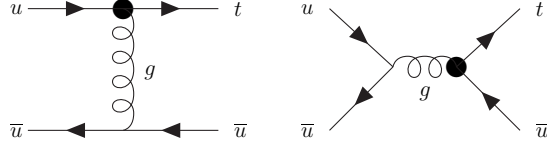


Figure A.3: Feynman diagram of process 3 for the strong sector.

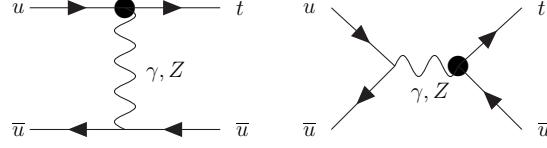


Figure A.4: Feynman diagram of process 3 for the electroweak sector.

Photon and Z interference

$$\begin{aligned}
\langle T_\gamma^t (T_z^t)^\dagger \rangle &= \frac{1}{4 \times 9} \frac{e^2 Q_c}{2t s_w c_w (t - m_z^2)} \text{Tr}[\delta] \text{Tr}[\delta] \\
&\quad \times \text{Tr}[(\not{p}_4 + m_t) \cdot V_\gamma^\beta(p_1, p_4, p_4 - p_1) \cdot \not{p}_1 \cdot \bar{V}_z^\alpha(p_1, p_4, p_4 - p_1)] \\
&\quad \times \text{Tr}[\not{p}_3 \cdot \gamma_\beta \cdot \not{p}_2 \cdot \bar{\Gamma}_\alpha(p_4 - p_1, Q_c)]. \quad (\text{A.10})
\end{aligned}$$

$$\begin{aligned}
\langle T_z^t (T_\gamma^t)^\dagger \rangle &= \frac{1}{4 \times 9} \frac{e^2 Q_c}{2t s_w c_w (t - m_z^2)} \text{Tr}[\delta] \text{Tr}[\delta] \\
&\quad \times \text{Tr}[(\not{p}_4 + m_t) \cdot V_z^\alpha(p_1, p_4, p_4 - p_1) \cdot \not{p}_1 \cdot \bar{V}_\gamma^\beta(p_1, p_4, p_4 - p_1)] \\
&\quad \times \text{Tr}[\not{p}_3 \Gamma_\alpha(p_4 - p_1, Q_c) \cdot \not{p}_2 \cdot \gamma_\beta]. \quad (\text{A.11})
\end{aligned}$$

A.2 Process 3

Process 3 is $u\bar{u} \rightarrow t\bar{u}$ (u coupling) (figures A.3 and A.4). As we can easily see this process has two channels, t and s. The transition amplitudes are

$$iT_g^t = [\bar{u}_t^i V_g^\mu(p_1, p_4, p_4 - p_1) 2t_{ij}^a u_1^j] \left(\frac{-ig_{\mu\nu}}{t} \right) [\bar{v}_3^k i g_3 t_{kl}^a \gamma^\nu v_2^l] \quad (\text{A.12})$$

$$iT_g^s = [\bar{u}_t^i V_g^\mu(-p_3, p_4, p_3 + p_4) 2t_{ij}^a v_3^j] \left(\frac{-ig_{\mu\nu}}{s} \right) [\bar{v}_2^k i g_3 t_{kl}^a \gamma^\nu u_1^l] \quad (\text{A.13})$$

$$iT_\gamma^t = [\bar{u}_t^i V_\gamma^\mu(p_1, p_4, p_4 - p_1) \delta_{ij} u_1^j] \left(\frac{-ig_{\mu\nu}}{t} \right) [\bar{v}_3^k i e Q_u \gamma^\nu \delta_{kl} v_2^l] \quad (\text{A.14})$$

$$iT_\gamma^s = [\bar{u}_t^i V_\gamma^\mu(-p_3, p_4, p_3 + p_4) \delta_{ij} v_3^j] \left(\frac{-ig_{\mu\nu}}{s} \right) [\bar{v}_2^k i e Q_u \gamma^\nu \delta_{kl} u_1^l] \quad (\text{A.15})$$

$$\begin{aligned} iT_Z^t &= [\bar{u}_t^i V_Z^\mu(p_1, p_4, p_4 - p_1) \delta_{ij} u_1^j] \left(\frac{-i}{t - m_z^2} \right) \left(g_{\mu\nu} - \frac{k_\mu k_\nu}{m_z^2} \right) \\ &\quad \left[\bar{v}_3^k \frac{ie}{\sin(2\theta_w)} \gamma_\nu [T_3 - 2Q_u^2 \sin^2(\theta_w) - T_3 \gamma_5] \delta_{kl} v_2^l \right] \end{aligned} \quad (\text{A.16})$$

$$\begin{aligned} iT_Z^s &= -[\bar{u}_t^i V_Z^\mu(-p_3, p_4, p_3 + p_4) \delta_{ij} v_3^j] \left(\frac{-i}{s - m_z^2} \right) \left(g_{\mu\nu} - \frac{k_\mu k_\nu}{m_z^2} \right) \\ &\quad \left[\bar{v}_2^k \frac{ie}{\sin(2\theta_w)} \gamma_\nu [T_3 - 2Q_u^2 \sin^2(\theta_w) - T_3 \gamma_5] \delta_{kl} u_1^l \right]. \end{aligned} \quad (\text{A.17})$$

And the total amplitude is

$$iT_{total} = iT_g^t + iT_g^s + iT_\gamma^t + iT_\gamma^s + iT_Z^t + iT_Z^s. \quad (\text{A.18})$$

Like before we present the spin and colour average

gluon

$$\begin{aligned} \langle T_g^t (T_g^t)^\dagger \rangle &= \frac{1}{4 \times 9} \frac{4g_3^2}{t^2} \text{Tr}[t^a t^b] \text{Tr}[t^a t^b] \\ &\quad \times \text{Tr}[V_g^\alpha(p_1, p_4, p_4 - p_1) \cdot \not{p}_1 \cdot \bar{V}_g^\beta(p_1, p_4, p_4 - p_1) \cdot (\not{p}_4 + m_t)] \\ &\quad \times \text{Tr}[\gamma_\alpha \cdot \not{p}_3 \cdot \gamma_\beta \cdot \not{p}_2] \end{aligned} \quad (\text{A.19})$$

$$\begin{aligned} \langle T_g^s (T_g^s)^\dagger \rangle &= \frac{1}{4 \times 9} \frac{4g_3^2}{s^2} \text{Tr}[t^a t^b] \text{Tr}[t^a t^b] \\ &\quad \times \text{Tr}[V_g^\alpha(-p_3, p_4, p_3 + p_4) \cdot \not{p}_3 \cdot \bar{V}_g^\beta(-p_3, p_4, p_3 + p_4) \cdot (\not{p}_4 + m_t)] \\ &\quad \times \text{Tr}[\gamma_\alpha \cdot \not{p}_1 \cdot \gamma_\beta \cdot \not{p}_2] \end{aligned} \quad (\text{A.20})$$

$$\begin{aligned} \langle T_g^t (T_g^s)^\dagger \rangle &= \frac{1}{4 \times 9} \frac{4g_3^2}{ts} \text{Tr}[t^a t^b t^a t^b] \\ &\quad \text{Tr}[\bar{V}_g^\alpha(-p_3, p_4, p_3 + p_4) \cdot (\not{p}_4 + m_t) \cdot V_g^\beta(p_1, p_4, p_4 - p_1) \cdot \\ &\quad \not{p}_1 \cdot \gamma_\alpha \cdot \not{p}_2 \cdot \gamma_\beta \cdot \not{p}_3] \end{aligned} \quad (\text{A.21})$$

$$\begin{aligned} \langle T_g^s (T_g^t)^\dagger \rangle &= \frac{1}{4 \times 9} \frac{4g_3^2}{ts} \text{Tr}[t^a t^b t^a t^b] \\ &\quad \text{Tr}[\bar{V}_g^\alpha(p_1, p_4, p_4 - p_1) \cdot (\not{p}_4 + m_t) \cdot V_g^\beta(-p_3, p_4, p_3 + p_4) \cdot \\ &\quad \not{p}_3 \cdot \gamma_\alpha \cdot \not{p}_2 \cdot \gamma_\beta \cdot \not{p}_1]. \end{aligned} \quad (\text{A.22})$$

Photon

$$\begin{aligned}
\langle T_\gamma^t (T_\gamma^t)^\dagger \rangle &= \frac{1}{4 \times 9} \left(\frac{eQ_u}{t} \right)^2 \text{Tr}[\delta] \text{Tr}[\delta] \\
&\times \text{Tr}[V_\gamma^\alpha(p_1, p_4, p_4 - p_1) \cdot \not{p}_1 \cdot \bar{V}_\gamma^\beta(p_1, p_4, p_4 - p_1) \cdot (\not{p}_4 + m_t)] \\
&\times \text{Tr}[\gamma_\alpha \cdot \not{p}_3 \cdot \gamma_\beta \cdot \not{p}_2]. \tag{A.23}
\end{aligned}$$

$$\begin{aligned}
\langle T_\gamma^u (T_\gamma^u)^\dagger \rangle &= \frac{1}{4 \times 9} \left(\frac{eQ_u}{s} \right)^2 \text{Tr}[\delta] \text{Tr}[\delta] \\
&\times \text{Tr}[V_\gamma^\alpha(-p_3, p_4, p_3 + p_4) \cdot \not{p}_3 \cdot \bar{V}_\gamma^\beta(-p_3, p_4, p_3 + p_4) \cdot (\not{p}_4 + m_t)] \\
&\times \text{Tr}[\gamma_\alpha \cdot \not{p}_1 \cdot \gamma_\beta \cdot \not{p}_2] \tag{A.24}
\end{aligned}$$

$$\begin{aligned}
\langle T_\gamma^t (T_\gamma^s)^\dagger \rangle &= \frac{1}{4 \times 9} \frac{(eQ_u)^2}{ts} \text{Tr}[\delta] \\
&\text{Tr}[V_\gamma^\alpha(p_1, p_4, p_4 - p_1) \cdot \not{p}_1 \cdot \gamma_\beta \cdot \not{p}_2 \cdot \gamma_\alpha \cdot \not{p}_3 \cdot \bar{V}_\gamma^\beta(-p_3, p_4, p_3 + p_4) \cdot \\
&(\not{p}_4 + m_t)] \tag{A.25}
\end{aligned}$$

$$\begin{aligned}
\langle T_\gamma^s (T_\gamma^t)^\dagger \rangle &= \frac{1}{4 \times 9} \frac{(eQ_u)^2}{ts} \text{Tr}[\delta] \\
&\text{Tr}[V_\gamma^\alpha(-p_3, p_4, p_3 + p_4) \cdot \not{p}_3 \cdot \gamma_\beta \cdot \not{p}_2 \cdot \gamma_\alpha \cdot \not{p}_1 \cdot \bar{V}_\gamma^\beta(p_1, p_4, p_4 - p_1) \cdot \\
&(\not{p}_4 + m_t)]. \tag{A.26}
\end{aligned}$$

Z

$$\begin{aligned}
\langle T_z^t (T_z^t)^\dagger \rangle &= \frac{1}{4 \times 9} \frac{e^2}{4s_w^2 c_w^2 (t - m_z^2)^2} \text{Tr}[\delta] \text{Tr}[\delta] \\
&\times \text{Tr}[V_Z^\alpha(p_1, p_4, p_4 - p_1) \cdot \not{p}_1 \cdot \bar{V}_Z^\beta(p_1, p_4, p_4 - p_1) \cdot (\not{p}_4 + m_t)] \\
&\times \text{Tr}[\Gamma_\alpha(p_4 - p_1, Q_u) \cdot \not{p}_3 \cdot \bar{\Gamma}_\beta(p_4 - p_1, Q_u) \cdot \not{p}_2] \tag{A.27}
\end{aligned}$$

$$\begin{aligned}
\langle T_z^s (T_z^s)^\dagger \rangle &= \frac{1}{4 \times 9} \frac{e^2}{4s_w^2 c_w^2 (s - m_z^2)^2} \text{Tr}[\delta] \text{Tr}[\delta] \\
&\times \text{Tr}[V_Z^\alpha(-p_3, p_4, p_3 + p_4) \cdot \not{p}_3 \cdot \bar{V}_Z^\beta(-p_3, p_4, p_3 + p_4) \cdot (\not{p}_4 + m_t)] \\
&\times \text{Tr}[\Gamma_\alpha(p_3 + p_4, Q_u) \cdot \not{p}_1 \cdot \bar{\Gamma}_\beta(p_3 + p_4, Q_u) \cdot \not{p}_2] \tag{A.28}
\end{aligned}$$

$$\begin{aligned}
\langle T_z^t(T_z^s)^\dagger \rangle &= \frac{1}{4 \times 9} \frac{e^2}{4s_w^2 c_w^2 (t - m_z^2)(s - m_z^2)} \text{Tr}[\delta] \\
&\times \text{Tr}[V_Z^\alpha(p_1, p_4, p_4 - p_1) \cdot \not{p}_1 \cdot \bar{\Gamma}_\beta(p_3 + p_4, Q_u) \not{p}_2 \cdot \Gamma_\alpha(p_4 - p_1, Q_u) \cdot \\
&\times \not{p}_3 \cdot \bar{V}_z^\beta(-p_3, p_4, p_3 + p_4) \cdot (\not{p}_4 + m_t)] \quad (\text{A.29})
\end{aligned}$$

$$\begin{aligned}
\langle T_z^s(T_z^t)^\dagger \rangle &= \frac{1}{4 \times 9} \frac{e^2}{4s_w^2 c_w^2 (t - m_z^2)(s - m_z^2)} \text{Tr}[\delta] \\
&\times \text{Tr}[V_Z^\alpha(-p_3, p_4, p_3 + p_4) \cdot \not{p}_3 \cdot \bar{\Gamma}_\beta(p_4 - p_1, Q_u) \not{p}_2 \cdot \Gamma_\alpha(p_3 + p_4, Q_u) \cdot \\
&\times \not{p}_1 \cdot \bar{V}_z^\beta(p_1, p_4, p_4 - p_1) \cdot (\not{p}_4 + m_t)]. \quad (\text{A.30})
\end{aligned}$$

Gluon and Photon interference

$$\begin{aligned}
\langle T_g^t(T_\gamma^s)^\dagger \rangle &= \frac{1}{4 \times 9} \frac{2eg_3 Q_u}{ts} \text{Tr}[t^a t^a] \\
&\times \text{Tr}[(\not{p}_4 + m_t) \cdot V_g^\alpha(p_1, p_4, p_4 - p_1) \cdot \not{p}_1 \cdot \gamma_\beta \cdot \not{p}_2 \cdot \gamma_\alpha \cdot \not{p}_3 \cdot \\
&\bar{V}_\gamma^\beta(-p_3, p_4, p_3 + p_4)] \quad (\text{A.31})
\end{aligned}$$

$$\begin{aligned}
\langle T_\gamma^s(T_g^t)^\dagger \rangle &= \frac{1}{4 \times 9} \frac{2eg_3 Q_u}{ts} \text{Tr}[t^a t^a] \\
&\times \text{Tr}[(\not{p}_4 + m_t) \cdot V_\gamma^\beta(-p_3, p_4, p_3 + p_4) \cdot \not{p}_3 \cdot \gamma_\alpha \cdot \not{p}_2 \cdot \gamma_\beta \cdot \not{p}_1 \cdot \\
&\bar{V}_g^\alpha(p_1, p_4, p_4 - p_1)] \quad (\text{A.32})
\end{aligned}$$

$$\begin{aligned}
\langle T_g^s(T_\gamma^t)^\dagger \rangle &= \frac{1}{4 \times 9} \frac{2eg_3 Q_u}{ts} \text{Tr}[t^a t^a] \\
&\times \text{Tr}[(\not{p}_4 + m_t) \cdot V_g^\alpha(-p_3, p_4, p_3 + p_4) \cdot \not{p}_3 \cdot \gamma_\beta \cdot \not{p}_2 \cdot \gamma_\alpha \cdot \not{p}_1 \cdot \\
&\bar{V}_\gamma^\beta(p_1, p_4, p_4 - p_1)] \quad (\text{A.33})
\end{aligned}$$

$$\begin{aligned}
\langle T_\gamma^t(T_g^s)^\dagger \rangle &= \frac{1}{4 \times 9} \frac{2eg_3 Q_u}{ts} \text{Tr}[t^a t^a] \\
&\times \text{Tr}[(\not{p}_4 + m_t) \cdot V_\gamma^\alpha(p_1, p_4, p_4 - p_1) \cdot \not{p}_1 \cdot \gamma_\beta \cdot \not{p}_2 \cdot \gamma_\alpha \cdot \not{p}_3 \cdot \\
&\bar{V}_g^\beta(-p_3, p_4, p_3 + p_4)] \quad (\text{A.34})
\end{aligned}$$

$$\langle T_g^t(T_\gamma^t)^\dagger \rangle = \langle T_\gamma^t(T_g^t)^\dagger \rangle = \langle T_g^s(T_\gamma^s)^\dagger \rangle = \langle T_\gamma^s(T_g^s)^\dagger \rangle = 0. \quad (\text{A.35})$$

Gluon and Z interference

$$\begin{aligned}
\langle T_g^t(T_z^s)^\dagger \rangle &= \frac{1}{4 \times 9} \frac{eg_3}{s_w c_w t (s - m_z^2)} Tr[t^a t^a] \\
&\times Tr[(\not{p}_4 + m_t) \cdot V_g^\alpha(p_1, p_4, p_4 - p_1) \cdot \not{p}_1 \cdot \bar{\Gamma}_\beta(p_3 + p_4, Q_u) \cdot \not{p}_2 \cdot \gamma_\alpha \cdot \not{p}_3 \cdot \\
&\bar{V}_z^\beta(-p_3, p_4, p_3 + p_4)] \quad (A.36)
\end{aligned}$$

$$\begin{aligned}
\langle T_z^s(T_g^t)^\dagger \rangle &= \frac{1}{4 \times 9} \frac{eg_3}{s_w c_w t (s - m_z^2)} Tr[t^a t^a] \\
&\times Tr[(\not{p}_4 + m_t) \cdot V_z^\beta(-p_3, p_4, p_3 + p_4, Q_u) \cdot \not{p}_3 \cdot \gamma_\alpha \cdot \not{p}_2 \cdot \Gamma_\beta(p_3 + p_4, Q_u) \cdot \not{p}_1 \cdot \\
&\bar{V}_g^\alpha(p_1, p_4, p_4 - p_1)] \quad (A.37)
\end{aligned}$$

$$\begin{aligned}
\langle T_g^s(T_z^t)^\dagger \rangle &= \frac{1}{4 \times 9} \frac{eg_3}{s_w c_w s (t - m_z^2)} Tr[t^a t^a] \\
&\times Tr[(\not{p}_4 + m_t) \cdot V_g^\beta(-p_3, p_4, p_3 + p_4) \cdot \not{p}_3 \cdot \bar{\Gamma}_\alpha(p_4 - p_1, Q_u) \cdot \not{p}_2 \cdot \gamma_\beta \cdot \not{p}_1 \cdot \\
&\bar{V}_z^\alpha(p_1, p_4, p_4 - p_1)] \quad (A.38)
\end{aligned}$$

$$\begin{aligned}
\langle T_z^t(T_g^s)^\dagger \rangle &= \frac{1}{4 \times 9} \frac{eg_3}{s_w c_w s (t - m_z^2)} Tr[t^a t^a] \\
&\times Tr[(\not{p}_4 + m_t) \cdot V_z^\alpha(p_1, p_4, p_4 - p_1) \cdot \not{p}_1 \cdot \gamma_\beta \cdot \not{p}_2 \cdot \Gamma_\alpha(p_4 - p_1, Q_u) \cdot \not{p}_3 \cdot \\
&\bar{V}_g^\beta(-p_3, p_4, p_3 + p_4)] \quad (A.39)
\end{aligned}$$

$$\langle T_g^t(T_z^t)^\dagger \rangle = \langle T_z^t(T_g^t)^\dagger \rangle = \langle T_g^s(T_z^s)^\dagger \rangle = \langle T_z^s(T_g^s)^\dagger \rangle = 0. \quad (A.40)$$

Photon and Z interference

$$\begin{aligned}
\langle T_\gamma^t(T_z^t)^\dagger \rangle &= \frac{1}{4 \times 9} \frac{e^2 Q_u}{2t s_w c_w (t - m_z^2)} Tr[\delta] Tr[\delta] \\
&\times Tr[(\not{p}_4 + m_t) \cdot V_\gamma^\alpha(p_1, p_4, p_4 - p_1) \cdot \not{p}_1 \cdot \bar{V}_z^\beta(p_1, p_4, p_4 - p_1)] \\
&\times Tr[\not{p}_2 \cdot \gamma_\alpha \cdot \not{p}_3 \cdot \bar{\Gamma}_\beta(p_4 - p_1, Q_u)] \quad (A.41)
\end{aligned}$$

$$\begin{aligned}
\langle T_\gamma^t(T_z^s)^\dagger \rangle &= \frac{1}{4 \times 9} \frac{e^2 Q_u}{2t s_w c_w (s - m_z^2)} Tr[\delta] \\
&\times Tr[(\not{p}_4 + m_t) \cdot V_\gamma^\alpha(p_1, p_4, p_4 - p_1) \cdot \not{p}_1 \cdot \bar{\Gamma}_\beta(p_3 + p_4, Q_u) \cdot \not{p}_2 \cdot \gamma_\alpha \cdot \not{p}_3 \cdot \\
&\bar{V}_z^\beta(-p_3, p_4, p_3 + p_4)] \quad (A.42)
\end{aligned}$$

$$\begin{aligned}
\langle T_\gamma^s(T_z^t)^\dagger \rangle &= \frac{1}{4 \times 9} \frac{e^2 Q_u}{2s s_w c_w (t - m_z^2)} \text{Tr}[\delta] \\
&\times \text{Tr}[(\not{p}_4 + m_t) \cdot V_\gamma^\alpha(-p_3, p_4, p_3 + p_4) \cdot \not{p}_3 \cdot \bar{\Gamma}_\beta(p_4 - p_1, Q_u) \cdot \not{p}_2 \cdot \gamma_\alpha \cdot \not{p}_1 \cdot \\
&\bar{V}_z^\beta(p_1, p_4, p_4 - p_1)] \quad (\text{A.43})
\end{aligned}$$

$$\begin{aligned}
\langle T_\gamma^s(T_z^s)^\dagger \rangle &= \frac{1}{4 \times 9} \frac{e^2 Q_u}{2s s_w c_w (s - m_z^2)} \text{Tr}[\delta] \text{Tr}[\delta] \\
&\times \text{Tr}[(\not{p}_4 + m_t) \cdot V_\gamma^\alpha(-p_3, p_4, p_3 + p_4) \cdot \not{p}_3 \cdot \bar{V}_z^\beta(-p_3, p_4, p_3 + p_4)] \\
&\times \text{Tr}[\not{p}_2 \cdot \gamma_\alpha \cdot \not{p}_1 \cdot \bar{\Gamma}_\beta(p_3 + p_4, Q_u)] \quad (\text{A.44})
\end{aligned}$$

$$\begin{aligned}
\langle T_z^t(T_\gamma^t)^\dagger \rangle &= \frac{1}{4 \times 9} \frac{e^2 Q_u}{2t s_w c_w (t - m_z^2)} \text{Tr}[\delta] \text{Tr}[\delta] \\
&\times \text{Tr}[(\not{p}_4 + m_t) \cdot V_z^\beta(p_1, p_4, p_4 - p_1) \cdot \not{p}_1 \cdot \bar{V}_\gamma^\alpha(p_1, p_4, p_4 - p_1)] \\
&\times \text{Tr}[\not{p}_2 \Gamma_\beta(p_4 - p_1, Q_u) \cdot \not{p}_3 \cdot \gamma_\alpha] \quad (\text{A.45})
\end{aligned}$$

$$\begin{aligned}
\langle T_z^t(T_\gamma^s)^\dagger \rangle &= \frac{1}{4 \times 9} \frac{e^2 Q_u}{2s s_w c_w (t - m_z^2)} \text{Tr}[\delta] \\
&\times \text{Tr}[(\not{p}_4 + m_t) \cdot V_z^\beta(p_1, p_4, p_4 - p_1) \cdot \not{p}_1 \cdot \gamma_\alpha \cdot \not{p}_2 \cdot \Gamma_\beta(p_4 - p_1, Q_u) \cdot \not{p}_3 \cdot \\
&\bar{V}_\gamma^\alpha(-p_3, p_4, p_3 + p_4)] \quad (\text{A.46})
\end{aligned}$$

$$\begin{aligned}
\langle T_z^s(T_\gamma^t)^\dagger \rangle &= \frac{1}{4 \times 9} \frac{e^2 Q_u}{2t s_w c_w (s - m_z^2)} \text{Tr}[\delta] \\
&\times \text{Tr}[(\not{p}_4 + m_t) \cdot V_z^\beta(-p_3, p_4, p_3 + p_4) \cdot \not{p}_3 \cdot \gamma_\alpha \cdot \not{p}_2 \cdot \Gamma_\beta(p_3 + p_4, Q_u) \cdot \not{p}_1 \cdot \\
&\bar{V}_\gamma^\alpha(p_1, p_4, p_4 - p_1)] \quad (\text{A.47})
\end{aligned}$$

$$\begin{aligned}
\langle T_z^s(T_\gamma^s)^\dagger \rangle &= \frac{1}{4 \times 9} \frac{e^2 Q_u}{2s s_w c_w (s - m_z^2)} \text{Tr}[\delta] \text{Tr}[\delta] \\
&\times \text{Tr}[(\not{p}_4 + m_t) \cdot V_z^\beta(-p_3, p_4, p_3 + p_4) \cdot \not{p}_3 \cdot \bar{V}_\gamma^\alpha(-p_3, p_4, p_3 + p_4)] \\
&\times \text{Tr}[\not{p}_2 \cdot \Gamma_\beta(p_3 + p_4, Q_u) \cdot \not{p}_1 \cdot \gamma_\alpha] \quad (\text{A.48})
\end{aligned}$$

A.3 Process 4

Process 4, $c\bar{c} \rightarrow t\bar{u}$ (u coupling), is a an s channel (figures A.5 and A.6). The transition amplitudes are

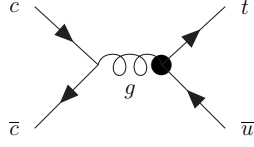


Figure A.5: Feynman diagram of process 4 for the strong sector.

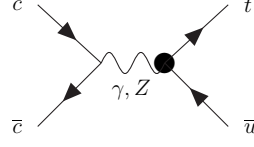


Figure A.6: Feynman diagram of process 4 for the electroweak sector.

$$iT_g^s = [\bar{u}_t^i V_g^\mu(-p_3, p_4, p_3 + p_4) 2t_{ij}^a v_3^j] \left(\frac{-ig_{\mu\nu}}{s} \right) [\bar{v}_2^k i g_3 t_{kl}^a \gamma^\nu u_1^l] \quad (\text{A.49})$$

$$iT_\gamma^s = [\bar{u}_t^i V_\gamma^\mu(-p_3, p_4, p_3 + p_4) \delta_{ij} v_3^j] \left(\frac{-ig_{\mu\nu}}{s} \right) [\bar{v}_2^k i e Q_c \gamma^\nu \delta_{kl} u_1^l] \quad (\text{A.50})$$

$$iT_Z^s = [\bar{u}_t^i V_Z^\mu(-p_3, p_4, p_3 + p_4) \delta_{ij} v_3^j] \left(\frac{-i}{s - m_Z^2} \right) (g_{\mu\nu} - \frac{k_\mu k_\nu}{m_Z^2}) [\bar{v}_2^k \frac{ie}{\sin(2\theta_w)} \gamma_\nu [T_3 - 2Q_c^2 \sin^2(\theta_w) - T_3 \gamma_5] \delta_{kl} u_1^l] \quad (\text{A.51})$$

and the total transition amplitude is

$$iT_{total} = iT_g^t + iT_\gamma^t + iT_Z^t. \quad (\text{A.52})$$

The total average is

gluon

$$\begin{aligned} \langle T_g^s (T_g^s)^\dagger \rangle &= \frac{1}{4 \times 9} \frac{4g_3^2}{s^2} Tr[t^a t^b] Tr[t^a t^b] \\ &\times Tr[V_g^\alpha(-p_3, p_4, p_3 + p_4) \cdot \not{p}_3 \cdot \bar{V}_g^\beta(-p_3, p_4, p_3 + p_4) \cdot (\not{p}_4 + m_t)] \\ &\times Tr[\gamma_\alpha \cdot \not{p}_1 \cdot \gamma_\beta \cdot \not{p}_2]. \end{aligned} \quad (\text{A.53})$$

Photon

$$\begin{aligned} \langle T_\gamma^s (T_\gamma^s)^\dagger \rangle &= \frac{1}{4 \times 9} \left(\frac{eQ_c}{s} \right)^2 Tr[\delta] Tr[\delta] \\ &\times Tr[V_\gamma^\alpha(-p_3, p_4, p_3 + p_4) \cdot \not{p}_3 \cdot \bar{V}_\gamma^\beta(-p_3, p_4, p_3 + p_4) \cdot (\not{p}_4 + m_t)] \\ &\times Tr[\gamma_\alpha \cdot \not{p}_1 \cdot \gamma_\beta \cdot \not{p}_2]. \end{aligned} \quad (\text{A.54})$$

Z

$$\begin{aligned}
\langle T_z^s(T_z^s)^\dagger \rangle &= \frac{1}{4 \times 9} \frac{e^2}{4s_w^2 c_w^2 (s - m_z^2)^2} \text{Tr}[\delta] \text{Tr}[\delta] \\
&\times \text{Tr}[V_Z^\alpha(-p_3, p_4, p_3 + p_4) \cdot \not{p}_3 \cdot \bar{V}_Z^\beta(-p_3, p_4, p_3 + p_4) \cdot (\not{p}_4 + m_t)] \\
&\times \text{Tr}[\Gamma_\alpha(p_3 + p_4, Q_c) \cdot \not{p}_1 \cdot \bar{\Gamma}_\beta(p_3 + p_4, Q_c) \cdot \not{p}_2]. \quad (\text{A.55})
\end{aligned}$$

Gluon and Photon interference

$$\langle T_g^s(T_\gamma^s)^\dagger \rangle = \langle T_\gamma^s(T_g^s)^\dagger \rangle = 0. \quad (\text{A.56})$$

Gluon and Z interference

$$\langle T_g^s(T_z^s)^\dagger \rangle = \langle T_z^s(T_g^s)^\dagger \rangle = 0. \quad (\text{A.57})$$

Photon and Z interference

$$\begin{aligned}
\langle T_\gamma^s(T_z^s)^\dagger \rangle &= \frac{1}{4 \times 9} \frac{e^2 Q_c}{2s s_w c_w (s - m_z^2)} \text{Tr}[\delta] \text{Tr}[\delta] \\
&\times \text{Tr}[(\not{p}_4 + m_t) \cdot V_\gamma^\beta(-p_3, p_4, p_3 + p_4) \cdot \not{p}_3 \cdot \bar{V}_z^\alpha(-p_3, p_4, p_3 + p_4)] \\
&\times \text{Tr}[\not{p}_2 \cdot \gamma_\beta \cdot \not{p}_1 \cdot \bar{\Gamma}_\alpha(p_3 + p_4, Q_c)] \quad (\text{A.58})
\end{aligned}$$

$$\begin{aligned}
\langle T_z^s(T_\gamma^s)^\dagger \rangle &= \frac{1}{4 \times 9} \frac{e^2 Q_c}{2s s_w c_w (s - m_z^2)} \text{Tr}[\delta] \text{Tr}[\delta] \\
&\times \text{Tr}[(\not{p}_4 + m_t) \cdot V_z^\alpha(-p_3, p_4, p_3 + p_4) \cdot \not{p}_3 \cdot \bar{V}_\gamma^\beta(-p_3, p_4, p_3 + p_4)] \\
&\times \text{Tr}[\not{p}_2 \Gamma_\alpha(p_3 + p_4, Q_c) \cdot \not{p}_1 \cdot \gamma_\beta]. \quad (\text{A.59})
\end{aligned}$$

A.4 Process 5

Process 5 is $u\bar{c} \rightarrow t\bar{c}$ (u coupling) (figure A.7 and A.8). This process is equivalent to process 2. The transition amplitudes for gluon, photon and Z respectively are

$$iT_g^t = [\bar{u}_t^i V_g^\mu(p_1, p_4, p_4 - p_1) 2t_{ij}^a u_1^j] \left(\frac{-ig_{\mu\nu}}{t} \right) [\bar{v}_2^k i g_3 t_{kl}^a \gamma^\nu v_3^l] \quad (\text{A.60})$$

$$iT_\gamma^t = [\bar{u}_t^i V_\gamma^\mu(p_1, p_4, p_4 - p_1) \delta_{ij} u_1^j] \left(\frac{-ig_{\mu\nu}}{t} \right) [\bar{v}_2^k i e Q_c \gamma^\nu \delta_{kl} v_3^l] \quad (\text{A.61})$$

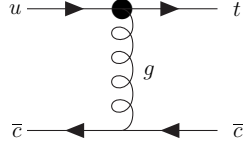


Figure A.7: Feynman diagram of process 5 for the strong sector.

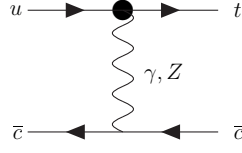


Figure A.8: Feynman diagram of process 5 for the electroweak sector.

$$\begin{aligned}
iT_Z^t &= [\bar{u}_t^i V_Z^\mu(p_1, p_4, p_4 - p_1) \delta_{ij} u_1^j] \left(\frac{-i}{t - m_z^2} \right) \left(g_{\mu\nu} - \frac{k_\mu k_\nu}{m_z^2} \right) \\
&\quad \left[\bar{v}_2^k \frac{ie}{\sin(2\theta_w)} \gamma_\nu [T_3 - 2Q_c^2 \sin^2(\theta_w) - T_3 \gamma_5] \delta_{kl} v_3^l \right]. \quad (\text{A.62})
\end{aligned}$$

The total transition amplitude is

$$iT_{total} = iT_g^t + iT_\gamma^t + iT_Z^t, \quad (\text{A.63})$$

and the average is

gluon

$$\begin{aligned}
\langle T_g^t (T_g^t)^\dagger \rangle &= \frac{1}{4 \times 9} \frac{4g_3^2}{t^2} Tr[t^{atb}] Tr[t^{atb}] \\
&\quad \times Tr[V_g^\alpha(p_1, p_4, p_4 - p_1) \cdot \not{p}_1 \cdot \bar{V}_g^\beta(p_1, p_4, p_4 - p_1) \cdot (\not{p}_4 + m_t)] \\
&\quad \times Tr[\gamma_\alpha \cdot \not{p}_3 \cdot \gamma_\beta \cdot \not{p}_2]. \quad (\text{A.64})
\end{aligned}$$

Photon

$$\begin{aligned}
\langle T_\gamma^t (T_\gamma^t)^\dagger \rangle &= \frac{1}{4 \times 9} \left(\frac{eQ_c}{t} \right)^2 Tr[\delta] Tr[\delta] \\
&\quad \times Tr[V_\gamma^\alpha(p_1, p_4, p_4 - p_1) \cdot \not{p}_1 \cdot \bar{V}_\gamma^\beta(p_1, p_4, p_4 - p_1) \cdot (\not{p}_4 + m_t)] \\
&\quad \times Tr[\gamma_\alpha \cdot \not{p}_3 \cdot \gamma_\beta \cdot \not{p}_2]. \quad (\text{A.65})
\end{aligned}$$

Z

$$\begin{aligned}
\langle T_z^t (T_z^t)^\dagger \rangle &= \frac{1}{4 \times 9} \frac{e^2}{4s_w^2 c_w^2 (t - m_z^2)^2} Tr[\delta] Tr[\delta] \\
&\quad \times Tr[V_Z^\alpha(p_1, p_4, p_4 - p_1) \cdot \not{p}_1 \cdot \bar{V}_Z^\beta(p_1, p_4, p_4 - p_1) \cdot (\not{p}_4 + m_t)] \\
&\quad \times Tr[\Gamma_\alpha(p_4 - p_1, Q_c) \cdot \not{p}_3 \cdot \bar{\Gamma}_\beta(p_4 - p_1, Q_c) \cdot \not{p}_2]. \quad (\text{A.66})
\end{aligned}$$

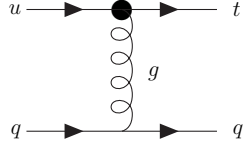


Figure A.9: FCNC Feynman diagram of process 7 for the strong sector.

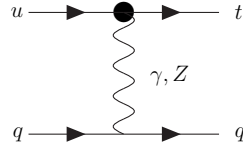


Figure A.10: FCNC Feynman diagram of process 7 for the electroweak sector.

Gluon and Photon interference

$$\langle T_g^t(T_\gamma^t)^\dagger \rangle = \langle T_\gamma^t(T_g^t)^\dagger \rangle = 0. \quad (\text{A.67})$$

Gluon and Z interference

$$\langle T_g^t(T_z^t)^\dagger \rangle = \langle T_z^t(T_g^t)^\dagger \rangle = 0. \quad (\text{A.68})$$

Photon and Z interference

$$\begin{aligned} \langle T_\gamma^t(T_z^t)^\dagger \rangle &= \frac{1}{4 \times 9} \frac{e^2 Q_c}{2t s_w c_w (t - m_z^2)} \text{Tr}[\delta] \text{Tr}[\delta] \\ &\quad \times \text{Tr}[(\not{p}_4 + m_t) \cdot V_\gamma^\beta(p_1, p_4, p_4 - p_1) \cdot \not{p}_1 \cdot \bar{V}_z^\alpha(p_1, p_4, p_4 - p_1)] \\ &\quad \times \text{Tr}[\not{p}_2 \cdot \gamma_\beta \cdot \not{p}_3 \cdot \bar{\Gamma}_\alpha(p_4 - p_1, Q_c)] \end{aligned} \quad (\text{A.69})$$

$$\begin{aligned} \langle T_z^t(T_\gamma^t)^\dagger \rangle &= \frac{1}{4 \times 9} \frac{e^2 Q_c}{2t s_w c_w (t - m_z^2)} \text{Tr}[\delta] \text{Tr}[\delta] \\ &\quad \times \text{Tr}[(\not{p}_4 + m_t) \cdot V_z^\alpha(p_1, p_4, p_4 - p_1) \cdot \not{p}_1 \cdot \bar{V}_\gamma^\beta(p_1, p_4, p_4 - p_1)] \\ &\quad \times \text{Tr}[\not{p}_2 \Gamma_\alpha(p_4 - p_1, Q_c) \cdot \not{p}_3 \cdot \gamma_\beta]. \end{aligned} \quad (\text{A.70})$$

A.5 Process 7

This process is described by $uq \rightarrow tq$, with q being a d, s or b quark (figures A.9 and A.10). As before we consider the SM diagram figure (A.11). The transition amplitudes for FCNC are

$$iT_g^t = [\bar{u}_t^i V_g^\mu(p_1, p_4, p_4 - p_1) 2t_{ij}^\alpha u_1^j] \left(\frac{-ig_{\mu\nu}}{t} \right) [\bar{u}_3^k i g_3 t_{kl}^a \gamma^\nu u_2^l] \quad (\text{A.71})$$

$$iT_\gamma^t = [\bar{u}_t^i V_\gamma^\mu(p_1, p_4, p_4 - p_1) \delta_{ij} u_1^j] \left(\frac{-ig_{\mu\nu}}{t} \right) [\bar{u}_3^k i e Q_d \gamma^\nu \delta_{kl} u_2^l] \quad (\text{A.72})$$

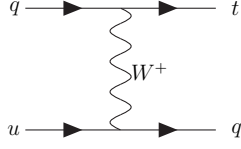


Figure A.11: SM Feynman diagram for process 7.

$$\begin{aligned}
iT_Z^t &= [\bar{u}_t^i V_z^\mu(p_1, p_4, p_4 - p_1) \delta_{ij} u_1^j] \left(\frac{-i}{t - m_z^2} \right) \left(g_{\mu\nu} - \frac{k_\mu k_\nu}{m_z^2} \right) \\
&\quad \left[\bar{u}_3^k \frac{ie}{\sin(2\theta_w)} \gamma_\nu [T_3 - 2Q_d^2 \sin^2(\theta_w) - T_3 \gamma_5] \delta_{kl} u_2^l \right]. \quad (\text{A.73})
\end{aligned}$$

For the SM diagram we have

$$\begin{aligned}
iT_W^t &= [\bar{u}_t^i i g \frac{\sqrt{2}}{2} \gamma^\mu \gamma_L V_{dt} \delta_{ij} u_2^j] \left(\frac{-i}{u - m_w^2} \right) \left(g_{\mu\nu} - \frac{k_\mu k_\nu}{m_w^2} \right) \\
&\quad \left[\bar{u}_3^k i g \frac{\sqrt{2}}{2} \gamma^\nu \gamma_L V_{du} \delta_{kl} u_1^l \right]. \quad (\text{A.74})
\end{aligned}$$

Like before the interferences are

Gluon and W interference

$$\begin{aligned}
\langle T_w^t (T_g^t)^\dagger \rangle &= \frac{1}{4 \times 9} \frac{i 2 g_3 g^2 V_{dt} V_{du}}{2t(u - m_w^2)} \text{Tr}[t^a t^a] \\
&\quad \times \text{Tr}[(\not{p}_4 + m_t) \cdot \gamma^\mu \cdot \gamma_L \cdot \not{p}_2 \cdot \gamma_\alpha \cdot \not{p}_3 \cdot F_\mu(p_4 - p_2) \cdot \not{p}_1 \cdot \\
&\quad \cdot \bar{V}_g^\alpha(p_1, p_4, p_4 - p_1)] \quad (\text{A.75})
\end{aligned}$$

$$\begin{aligned}
\langle T_g^t (T_w^t)^\dagger \rangle &= \frac{1}{4 \times 9} \frac{-i 2 g_3 g^2 V_{dt}^* V_{du}^*}{2t(u - m_w^2)} \text{Tr}[t^a t^a] \\
&\quad \times \text{Tr}[(\not{p}_4 + m_t) \cdot V_g^\alpha(p_1, p_4, p_4 - p_1) \cdot \not{p}_1 \cdot \bar{F}_\mu(p_4 - p_2) \cdot \\
&\quad \cdot \not{p}_3 \cdot \gamma_\alpha \cdot \not{p}_2 \cdot \gamma_R \cdot \gamma^\mu]. \quad (\text{A.76})
\end{aligned}$$

Photon and W interference

$$\begin{aligned}
\langle T_w^t (T_\gamma^t)^\dagger \rangle &= \frac{1}{4 \times 9} \frac{ieg^2 V_{dt} V_{du} Q_d}{2t(u - m_w^2)} \text{Tr}[\delta] \\
&\times \text{Tr}[(\not{p}_4 + m_t) \cdot \gamma^\mu \cdot \gamma_L \cdot \not{p}_2 \cdot \gamma_\alpha \cdot \not{p}_3 \cdot F_\mu(p_4 - p_2) \cdot \not{p}_1 \cdot \\
&\cdot \bar{V}_\gamma^\alpha(p_1, p_4, p_4 - p_1)] \quad (\text{A.77})
\end{aligned}$$

$$\begin{aligned}
\langle T_\gamma^t (T_w^t)^\dagger \rangle &= \frac{1}{4 \times 9} \frac{-ieg^2 V_{dt}^* V_{du}^* Q_d}{2t(u - m_w^2)} \text{Tr}[\delta] \\
&\times \text{Tr}[(\not{p}_4 + m_t) \cdot V_\gamma^\alpha(p_1, p_4, p_4 - p_1) \cdot \not{p}_1 \cdot \bar{F}_\mu(p_4 - p_2) \cdot \\
&\not{p}_3 \cdot \gamma_\alpha \cdot \not{p}_2 \cdot \gamma_R \cdot \gamma^\mu]. \quad (\text{A.78})
\end{aligned}$$

Z and W interference

$$\begin{aligned}
\langle T_w^t (T_z^t)^\dagger \rangle &= \frac{1}{4 \times 9} \frac{ieg^2 V_{dt} V_{du}}{4(t - m_z^2)(u - m_w^2) s_w c_w} \text{Tr}[\delta] \\
&\times \text{Tr}[(\not{p}_4 + m_t) \cdot \gamma^\mu \cdot \gamma_L \cdot \not{p}_2 \cdot \bar{\Gamma}_\alpha(p_4 - p_1) \cdot \not{p}_3 \cdot F_\mu(p_4 - p_2) \cdot \not{p}_1 \cdot \\
&\cdot \bar{V}_z^\alpha(p_1, p_4, p_4 - p_1)] \quad (\text{A.79})
\end{aligned}$$

$$\begin{aligned}
\langle T_z^t (T_w^t)^\dagger \rangle &= \frac{1}{4 \times 9} \frac{-ieg^2 V_{dt}^* V_{du}^*}{4(t - m_z^2)(u - m_w^2) s_w c_w} \text{Tr}[\delta] \\
&\times \text{Tr}[(\not{p}_4 + m_t) \cdot V_z^\alpha(p_1, p_4, p_4 - p_1) \cdot \not{p}_1 \cdot \bar{F}_\mu(p_4 - p_2) \cdot \\
&\not{p}_3 \cdot \Gamma_\alpha(p_4 - p_1, Q_d) \cdot \not{p}_2 \cdot \gamma_R \cdot \gamma^\mu]. \quad (\text{A.80})
\end{aligned}$$

A.6 Process 8

This process is described by $u\bar{q} \rightarrow t\bar{q}$, with \bar{q} being a d, s or d quark (figures A.12 and A.13). The SM diagram is shown in figure (A.14). The transition amplitudes for FCNC are

$$iT_g^t = [\bar{u}_t^i V_g^\mu(p_1, p_4, p_4 - p_1) 2t_{ij}^a u_1^j] \left(\frac{-ig_{\mu\nu}}{t} \right) [\bar{v}_2^k i g_3 t_{kl}^a \gamma^\nu v_3^l] \quad (\text{A.81})$$

$$iT_\gamma^t = [\bar{u}_t^i V_\gamma^\mu(p_1, p_4, p_4 - p_1) \delta_{ij} u_1^j] \left(\frac{-ig_{\mu\nu}}{t} \right) [\bar{v}_2^k i e Q_d \gamma^\nu \delta_{kl} v_3^l] \quad (\text{A.82})$$

$$\begin{aligned}
iT_Z^t &= [\bar{u}_t^i V_z^\mu(p_1, p_4, p_4 - p_1) \delta_{ij} u_1^j] \left(\frac{-i}{t - m_z^2} \right) (g_{\mu\nu} - \frac{k_\mu k_\nu}{m_z^2}) \\
&[\bar{v}_2^k \frac{ie}{\sin(2\theta_w)} \gamma_\nu [T_3 - 2Q_d^2 \sin^2(\theta_w) - T_3 \gamma_5] \delta_{kl} v_3^l]. \quad (\text{A.83})
\end{aligned}$$

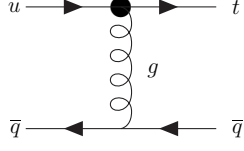


Figure A.12: FCNC Feynman diagram of process 8 for the strong sector.

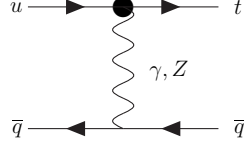


Figure A.13: FCNC Feynman diagram of process 8 for the electroweak sector.

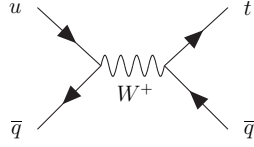


Figure A.14: SM Feynman diagram for process 8.

For the SM diagram we have

$$\begin{aligned}
 iT_W^t &= [\bar{u}_i^j ig \frac{\sqrt{2}}{2} \gamma^\mu \gamma_L V_{dt} \delta_{ij} v_3^j] \left(\frac{-i}{s - m_w^2} \right) \left(g_{\mu\nu} - \frac{k_\mu k_\nu}{m_w^2} \right) \\
 &\quad [\bar{v}_2^k ig \frac{\sqrt{2}}{2} \gamma^\nu \gamma_L V_{du} \delta_{kl} u_1^l].
 \end{aligned} \tag{A.84}$$

The interferences are

Gluon and W interference

$$\begin{aligned}
 \langle T_w^s (T_g^t)^\dagger \rangle &= \frac{1}{4 \times 9} \frac{i2g_3 g^2 V_{dt} V_{du}}{2t(s - m_w^2)} Tr[t^a t^a] \\
 &\quad \times Tr[(\not{p}_4 + m_t) \cdot \gamma^\mu \cdot \gamma_L \cdot \not{p}_3 \cdot \gamma_\alpha \cdot \not{p}_2 \cdot F_\mu(p_3 + p_4) \cdot \not{p}_1 \cdot \\
 &\quad \cdot \bar{V}_g^\alpha(p_1, p_4, p_4 - p_1)]
 \end{aligned} \tag{A.85}$$

$$\begin{aligned}
 \langle T_g^t (T_w^s)^\dagger \rangle &= \frac{1}{4 \times 9} \frac{-i2g_3 g^2 V_{dt}^* V_{du}^*}{2t(s - m_w^2)} Tr[t^a t^a] \\
 &\quad \times Tr[(\not{p}_4 + m_t) \cdot V_g^\alpha(p_1, p_4, p_4 - p_1) \cdot \not{p}_1 \cdot \bar{F}_\mu(p_3 + p_4) \cdot \\
 &\quad \cdot \not{p}_2 \cdot \gamma_\alpha \cdot \not{p}_3 \cdot \gamma_R \cdot \gamma^\mu].
 \end{aligned} \tag{A.86}$$

Photon and W interference

$$\begin{aligned}
\langle T_w^s(T_\gamma^t)^\dagger \rangle &= \frac{1}{4 \times 9} \frac{ieg^2 V_{dt} V_{du} Q_d}{2t(s - m_w^2)} Tr[\delta] \\
&\times Tr[(\not{p}_4 + m_t) \cdot \gamma^\mu \cdot \gamma_L \cdot \not{p}_3 \cdot \gamma_\alpha \cdot \not{p}_2 \cdot F_\mu(p_3 + p_4) \cdot \not{p}_1 \cdot \\
&\cdot \bar{V}_\gamma^\alpha(p_1, p_4, p_4 - p_1)] \quad (A.87)
\end{aligned}$$

$$\begin{aligned}
\langle T_\gamma^t(T_w^s)^\dagger \rangle &= \frac{1}{4 \times 9} \frac{-ieg^2 V_{dt}^* V_{du}^* Q_d}{2t(s - m_w^2)} Tr[\delta] \\
&\times Tr[(\not{p}_4 + m_t) \cdot V_\gamma^\alpha(p_1, p_4, p_4 - p_1) \cdot \not{p}_1 \cdot \bar{F}_\mu(p_3 + p_4) \cdot \\
&\not{p}_2 \cdot \gamma_\alpha \cdot \not{p}_3 \cdot \gamma_R \cdot \gamma^\mu]. \quad (A.88)
\end{aligned}$$

Z and W interference

$$\begin{aligned}
\langle T_w^s(T_z^t)^\dagger \rangle &= \frac{1}{4 \times 9} \frac{ieg^2 V_{dt} V_{du}}{4(t - m_z^2)(s - m_w^2) s_w c_w} Tr[\delta] \\
&\times Tr[(\not{p}_4 + m_t) \cdot \gamma^\mu \cdot \gamma_L \cdot \not{p}_3 \cdot \bar{\Gamma}_\alpha(p_4 - p_1) \cdot \not{p}_2 \cdot F_\mu(p_3 + p_4) \cdot \not{p}_1 \cdot \\
&\cdot \bar{V}_z^\alpha(p_1, p_4, p_4 - p_1)] \quad (A.89)
\end{aligned}$$

$$\begin{aligned}
\langle T_z^t(T_w^s)^\dagger \rangle &= \frac{1}{4 \times 9} \frac{-ieg^2 V_{dt}^* V_{du}^*}{4(t - m_z^2)(s - m_w^2) s_w c_w} Tr[\delta] \\
&\times Tr[(\not{p}_4 + m_t) \cdot V_z^\alpha(p_1, p_4, p_4 - p_1) \cdot \not{p}_1 \cdot \bar{F}_\mu(p_3 + p_4) \cdot \\
&\not{p}_2 \cdot \Gamma_\alpha(p_4 - p_1, Q_d) \cdot \not{p}_3 \cdot \gamma_R \cdot \gamma^\mu]. \quad (A.90)
\end{aligned}$$

Appendix B

Mathematica

All calculations had as fundamental tool the software Mathematica 5.2 with the package designed to particle physics calculations, FeynCalc [17]. We used this package in the first stage of the calculation process to analytically calculate the traces from the transition amplitudes. We also used Mathematica 5.2 for the second part, the integration of the differential cross sections. Finally this software was extremely useful to produce simplification on the expressions and, since it is programmable, to organize all calculations.

B.0.1 Transition amplitudes calculations

In figure(B.2) a typically Mathematica file for the transition amplitudes calculations is shown. This file is where we calculated the average of the square transition amplitudes for the gluon channel in process 1. It is separated in six sections. The first one defines the momentum variables. In the present case we worked with five momentums, four for the particles and one for the propagator. In the next two sections we defined two functions, $Vg(\alpha, p_i, p_j, k)$ and $Vgadj(\alpha, p_i, p_j, k) = \gamma^0 Vg(\alpha, p_i, p_j, k)^\dagger \gamma^0$, which are the FCNC vertices, and the kinematical constraints of the problem. The following section is where the traces are calculated. In figure (B.1) the form of one of the trace calculation is shown. Here p_i are the particle's momentum and the p_{isl} are the momentum contracted with gamma matrices, \not{p}_i . $Vg(\alpha, p_i, p_j, k)$ are functions defined earlier, $GA[\alpha]$ is the gamma matrix and $Tr[]$ is the function from FeynCalc that calculates the traces. After this first stage the results will pass through the section "Anomalous couplings". Here it is verified for all terms resulted from the previous calculations, which of the possible combinations of anomalous couplings have associated. With this information stored we have the final section "Results", that will orga-

 $T_g^t(T_g^t)^*$

```
A1 = Vg[α, p1, p4, k1].p1s1.Vgadg[τ, p1, p4, k1].(p4s1 + mt);  
B1 = GA[α].p2s1.GA[τ].p3s1;  
resultado1 = FullSimplify[ $\frac{4 g^3^2}{4 * t^2} * c1 * \text{Contract}[\text{Tr}[\mathbf{A1}] * \text{Tr}[\mathbf{B1}]]$ ];
```

Figure B.1: Trace calculation section.

nize and print all the expressions in the order defined above (F1, F2, etc.) with the respective anomalous couplings.

B.0.2 PDF integration

In figure (B.4) the file where the results for process 1 are convoluted and integrated with the PDF functions is shown. As we can see the file is divided in seven sections. The first two define the expressions obtained before, the value of the constants and the kinematic limits for the integrations. The third section is where the first integration is made. In our case it is the integration of the Mandelstam variable t . From equation (4.2) the limits of this integration will depend of the s variable. The fourth section is where the PDF functions are loaded and in the fifth section we define the kinematic limit for the s variable through equation (4.2). We also define a step function. This function is necessary for the second integration since we will be running the variables, x_1 and x_2 , from zero to one, which means that for a range of values the relations $s = x_1 x_2 S$ will outrange the kinematics limits for s , s_{min} . Therefore we define for these domains the value of zero so that there won't be any contribution. The sixth section is where the integration of the s variable is made. In figure (B.5) we can see its form. In the bold text we have the information of the PDF function load by the PDF package. The integration is made by the command `NIntegrate()`, which calculates a numerical integration of the expressions resulted from the first integration, convoluted with the PDF functions. We can see that for this case (process 1) we worked with two quarks u . Finally the last section will organize and print all results. It is also here that we multiply the final result with a units conversion factor and with, in case of existence, a combinatorial factor. Except for process 1 this factor is always 2.

uu_tu_(1)_g.nb

<< HighEnergyPhysics`FeynCalc`

Momentum definition

Vertices

Scalar constrains

Trace calculations

$T_g^t (T_g^t)^*$

$T_g^u (T_g^u)^*$

$T_g^t (T_g^u)^*$

$T_g^u (T_g^t)^*$

Anomalous couplings

Results

Figure B.2: Mathematica file for gluon channel of process 1.

Results

```
If[count2 / 2 ∈ Integers, Print["Erro!!!!!"]]

count3 = 1;
Do[
  If[lista2[i] == 1,
    str = ToString[count3];
    str = "F" <> qaz;
    StylePrint[listacoeff[i] str, "Input"];
    StylePrint[lista[i] // StandardForm, "Input"];
    count3 = count3 + 1;]
, {i, 1, 15}]

count4 = 16;
Do[
  marca = count4 + j;
  Do[
    If[lista2[k] == 1,
      Do[
        stop = 0;
        If[lista2[l] == 1,
          primeirotermo = lista[k];
          segundotermo = lista[l];
          divisao = Simplify[primeirotermo / segundotermo];
          If[divisao == 1,
            str = ToString[count3];
            str = "MF" <> str;
            StylePrint[listacoeff2[k, 1] str, "Input"];
            StylePrint[2 * (lista[k]) // StandardForm, "Input"];
            marca = 1 + 1;
            count3 = count3 + 1;
            Break[];
          ];
          If[divisao == -1,
            str = ToString[count3];
            str = "MF" <> str;
            StylePrint[listacoeff2[k, 2] str, "Input"];
            StylePrint[2 * i * (lista[k]) // StandardForm, "Input"];
            marca = 1 + 1;
            count3 = count3 + 1;
            Break[];
          ];
        ];
      ], {l, marca, count4 + 2 * j - 1}];
    ], {k, count4, count4 + j - 1};
  count4 = count4 + 2 * j;
  ], {j, 29, 1, -2}]
```

Figure B.3: Section of amplitudes calculation results.

Expressions

Constants and limits definitions

First integration

Load PDF

Definitions of s minimum and Step function

Second integration

Results

Figure B.4: Mathematica file of the PDF integration for *process1*.

Second integration

Expression style:

$$\iint dx_1 dx_2 \text{ pdf}[a,b,x_i,Q^2] \text{ pdf}[c,d,x_j,Q^2] \sigma(u_1 u_2 \rightarrow t \ x)$$

a : Defines CTEQ

b: Definesn the parton:

```
-6= "t-bar quark";
-5= "b-bar quark";
-4= "c-bar quark";
-3= "s-bar quark";
-2= "d-bar quark";
-1= "u-bar quark";
0= "gluon";
1= "u quark";
2= "d quark";
3= "s quark";
4= "c quark";
5= "b quark";
6= "t quark";
```

xi: variable defined by $P_{\text{quark } i} = \text{xi} * P_{\text{protão}}$

Q : Energy scale (175 in our case)

```
Array[listasigmaint, 66];
Do[
  j = i;
  listasigmaint[i] = NIntegrate[listasigma[j] * pdf[1, 1, x1, mt] * pdf[1, 1, x2, mt],
    {x1, 0.0001, 1}, {x2, 0.0001, 1}];
  Print[j, " ", "integral ok"];
  , {i, 1, 66}];
```

Figure B.5: Second integration section of the PDF integration.

Appendix C

Standard Model Feynman Rules

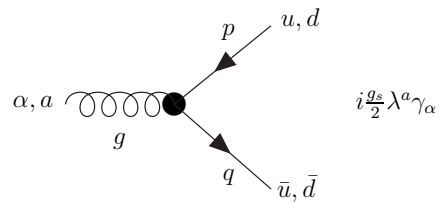


Figure C.1: Feynman rules for the SM $\bar{u}ug$ and $\bar{d}dg$ vertices. λ^a are the Gell-Mann matrices normalized such as $Tr(\lambda^a\lambda^b) = 2\delta^{ab}$.

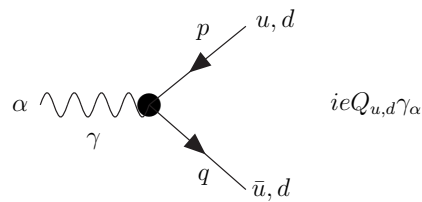


Figure C.2: Feynman rules for the SM $\bar{u}u\gamma$ and $\bar{d}d\gamma$ vertices.

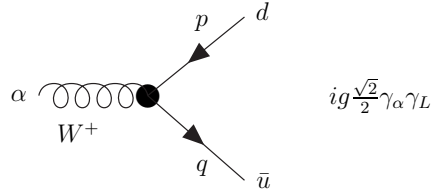


Figure C.3: Feynman rules for the SM $\bar{u}dW^+$ vertex.

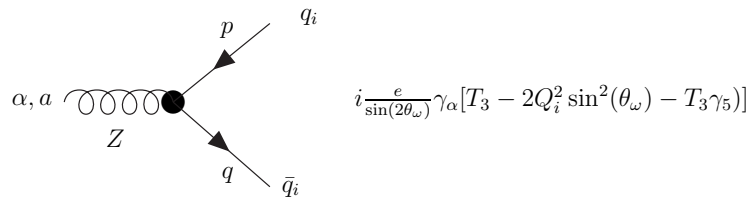


Figure C.4: Feynman rules for the SM $\bar{u}uZ$ and $\bar{d}dZ$ vertices. $T_3 = 1/2$ for up-type quarks and $T_3 = -1/2$ for down-type quarks

Bibliography

- [1] P. M. Ferreira, O. Oliveira, and R. Santos. Flavour changing strong interaction effects on top quark physics at the LHC. *Phys. Rev.*, D73:034011, 2006.
- [2] P. M. Ferreira and R. Santos. Strong flavour changing effective operator contributions to single top quark production. *Phys. Rev.*, D73:054025, 2006.
- [3] P. M. Ferreira and R. Santos. Contributions from dimension six strong flavor changing operators to t anti-t, t plus gauge boson, and t plus Higgs boson production at the LHC. *Phys. Rev.*, D74:014006, 2006.
- [4] J. A. Aguilar-Saavedra. Top flavour-changing neutral interactions: Theoretical expectations and experimental detection. *Acta Phys. Polon.*, B35:2695–2710, 2004.
- [5] F. del Aguila et al. Collider aspects of flavour physics at high Q. 2008.
- [6] H. Georgi. *Annual Review of Nuclear and Particle Science*, 43:209 (1993).
- [7] W. Buchmuller and D. Wyler. Effective Lagrangian Analysis of New Interactions and Flavor Conservation. *Nucl. Phys.*, B268:621, 1986.
- [8] P. M. Ferreira, R. B. Guedes, and R. Santos. Combined effects of strong and electroweak FCNC effective operators in top quark physics at the LHC. *Phys. Rev.*, D77:114008, 2008.
- [9] <http://www.phys.psu.edu/cteq/>.
- [10] J. Pumplin et al. New generation of parton distributions with uncertainties from global QCD analysis. *JHEP*, 07:012, 2002.
- [11] <http://durpdg.dur.ac.uk/hepdata/pdf3.html>.

- [12] W. M. Yao et al. Review of particle physics. *J. Phys.*, G33:1–1232, 2006.
- [13] Zack Sullivan. Understanding single-top-quark production and jets at hadron colliders. *Phys. Rev.*, D70:114012, 2004.
- [14] John Campbell, R. Keith Ellis, and Francesco Tramontano. Single top production and decay at next-to-leading order. *Phys. Rev.*, D70:094012, 2004.
- [15] John Campbell and Francesco Tramontano. Next-to-leading order corrections to $W t$ production and decay. *Nucl. Phys.*, B726:109–130, 2005.
- [16] J. Carvalho et al. Study of ATLAS sensitivity to FCNC top decays. *Eur. Phys. J.*, C52:999–1019, 2007.
- [17] R. Mertig, M. Bohm, and Ansgar Denner. FEYN CALC: Computer algebraic calculation of Feynman amplitudes. *Comput. Phys. Commun.*, 64:345–359, 1991.